Fleischner Lecture

Biokinetic Impacts on Structure and Imaging of the Lung: The Concept of Biologically Closed Electric Circuits

Björn E. W. Nordenström[1]

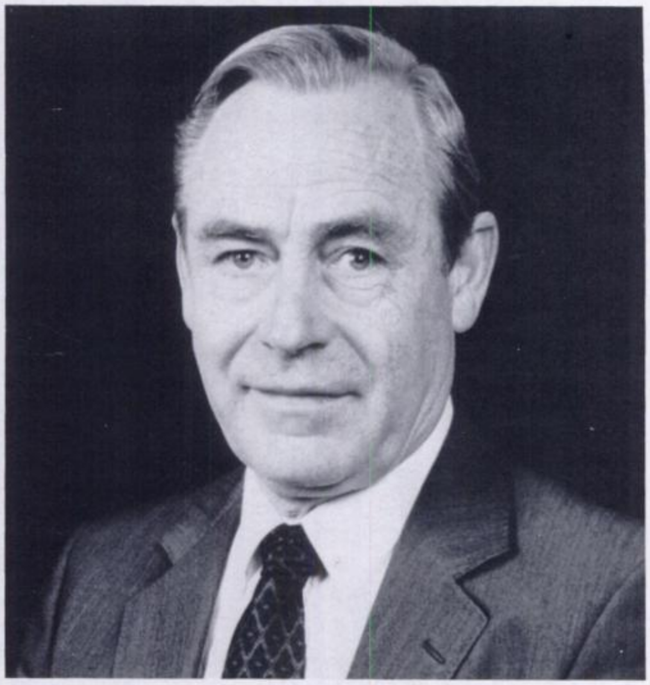

The *corona complex* of the lung is a collection of radiographic features surrounding a pulmonary mass. Each of its 12 components may be explained by a recently described subset of biologically closed electric circuits, the *vascular-interstitial closed electric circuit* (VICC) system. This system is activated both by normal metabolism of tissue and by local degrading processes, such as spontaneous necrosis or hemorrhage, that lead to local electrochemical polarization of a lesion in relation to surrounding noninjured tissue. Ions, cells, and water are transported electrically in the VICC system, leading to the development of the corona complex. The VICC system is conceived to exist with the walls of arteries and veins functioning as insulators around the electrically conducting medium of blood, the plasma. Blood vessels therefore connect electrically the injured and noninjured tissues. At the capillary level, electric junctions connect plasma and interstitial fluid, which functions as an electrical conductor comparable to blood plasma. The interstitial fluid therefore completes the circuit. The VICC system can be regarded as an additional circulatory system for selective electrogenic transports, coupled directly to the mechanical circulation of blood and lymph. The injury potential represents an important energetic factor in the activation of the VICC system. It is a slowly fluctuating, attenuating, electrochemical potential inducing ebb and flow of time-dependent anionic and cationic transports. The corona structures are special effects of the healing of injured tissue. The 12 radiologic signs of the corona complex have each been produced experimentally in vitro in animals and in vivo in humans during electrochemical treatment of cancers. The *"A" zone* is characterized radiographically by radiolucency around an electrically polarizing focal lesion. Peripheral to the A zone, a *"B" zone* is seen as a radiopaque region. The A and B zones are predominantly the result of an electroosmotic outflow of water from a lesion during its electropositive phase. At the interface between the A and B zones, *small arches* sometimes form an *arcade*. This configuration develops when the polarizing lesion has small protrusions at its surface. As a result of electrical edge enhancement, various elements of the interstitial tissue are transformed into *radiating fibrous structures*. They grow out at right angles to the surface of the lesion and serve as supporting columns for the arches. When necrotic material from a tumor is evacuated through a bronchus, ensuing collapse of the tumor will displace those radiating structures already produced. They then present as irregular elongated opacities termed *lamellae*. Experimental production of A and B zones, the radiating

---

Received September 7, 1984; accepted after revision April 17, 1985.
Presented at the annual meeting of the Fleischner Society, Santa Fe, NM, June 1984.

[1] Department of Diagnostic Radiology, Karolinska Hospital, P.O. Box 60 500, S-104 01 Stockholm, Sweden.

AJR 145:447–467, September 1985 0361–803X/85/1453–0447 © American Roentgen Ray Society

structures, and arches and arcades is presented. *Circumferential structures* are described as partly caused by *perifocal emphysema* due to dystrophic changes in the lung parenchyma by microthromboses of vessels around a lesion. *Perifocal edema*, caused by an electroosmotic inflow of water to the mass during its electronegative phase, may also contribute to a circular displacement of structures. *Interlobular edema* develops when the degrading process is electropositive and water accumulates by stasis peripheral to the tumor. Retraction of fibrous tissue is demonstrated experimentally as an effect of local dehydration by electroosmosis, leading to shrinkage of hydrophilic elastic fibrous tissue. This mechanism also produces a structural change, *retraction pocket* of the pleura, which was found to be equivalent to the retraction of skin and so-called skin thickening adjacent to breast cancers. *Calcifications* in tissue represent an internal modification of polarizing masses. By applying a fluctuating potential to normal human fat tissue specimens, typical microcalcifications have been produced. Pathologic tissue calcifications, developed after injury, may not be regarded as a disease per se but as a part of the healing process.

The process of radiologic diagnosis often is initially descriptive, followed by anatomic and functional correlations. Insight into the diagnostic and prognostic meaning of radiologic observations is, however, suboptimal until the underlying biologic mechanisms for their development are understood. I describe the corona structures of the lung, which together may be called the *corona complex.* Studies of their pathogenesis have led to a new biophysical concept capable of explaining their origin, the *vascular-interstitial closed electric circuit* (VICC) system.

In a paper 15 years ago [1], I described some structural elements seen around cancers of the lung. The radiographic appearance of these peritumoral features in many respects resembles the corona of the sun. I therefore tentatively called the constellation of these structures the *corona maligna.* The incidence of coronalike structures around lung cancers has been roughly 30% in my experience with 7000 cases but, as I later found, they are not specific for cancers. They can also be seen around benign tumors and granulomas. Therefore, the term *corona maligna* should no longer be used. A new term, *corona radiata*, appeared later in the literature. However, *corona radiata* is already an accepted term for the projection fibers between the cortex and the base of the brain. It is also sometimes used for structures in the ovary. To avoid confusion, this term should be abandoned for lung lesions. Furthermore, *corona radiata* refers to radiating structures, which represent only one of several radiographically observable corona structures. All of the corona structures, however, can be tied to a common biokinetic mechanism for their development. The constellation of the various corona structures may be called the *corona complex* [2].

The corona structures are observed around various lesions in the lung, but also in modified form in other organs (e.g., brain, liver, and breast). The 12 corona structures are the "A" zone, "B" zone, radiating structures, arches and arcades, lamellae, circumferential structures, narrowing of vessels, perifocal emphysema, perifocal edema, interlobular edema, fibrous tissue including retraction pockets and retraction edema, and calcifications. They develop under the influence of dynamically changing electrokinetic forces in a newly defined biokinetic transport mechanism called the vascular interstitial closed electric circuit (VICC) [2, pp. 122–172]. The VICC is activated under physiologic conditions by metabolic polarization among various tissues and by tissue injury (focal necrosis, bleeding, infection) in cancers, benign neoplasms, and granulomas. Variation in tissue injury explains the appearance of corona structures around some but not all lesions. The dynamic changes in activation of the VICC system lead to the time-dependent appearance of structural elements (i.e., several may appear nonsimultaneously). Structuring within the corona complex is influenced also by molecular, hydrostatic, and mechanical forces [2, pp. 75–78, 93–111].

In spite of the disparate radiologic appearances of the individual corona structures, they are largely dependent on an activated VICC. The general structure and function of this biokinetic system will be surveyed before each of the individual corona structures is described.

The Vascular-Interstitial Closed Electric Circuit

The circulation of blood provides transport of materials to various tissues in a mechanical manner. At the level of the capillaries, the materials enter tissue selectively by filtration, diffusion, and differences in colloid osmotic pressures over the capillary membranes. The VICC is involved in selective, electrogenous transports between blood and tissue. It therefore represents an additional circulatory system, coupled directly to the circulation of blood and lymph. The activation and construction of the VICC system are conceived as follows:

Activation of the VICC System

Local anabolic or catabolic processes produce electrochemical (i.e., physicochemical) polarization of tissue. For example, a person senses a working muscle as tired because lactic acid accumulates in it; that is, a metabolic, electrochemical gradient is produced in the muscle in relation to surrounding tissues. The process of degradation in an injured tissue releases catabolic energy, which is identified by an electrochemical injury potential when measured in relation to surrounding noninjured tissue.

The presence of an electric injury potential was demonstrated in various pulmonary lesions in 107 patients by the use of electrodes inserted by modified techniques for percutaneous needle biopsy [2, pp. 46–48; 3]. A profile of electric potential was traced through the lesions and surrounding tissues and measured in relation to a grounded subcutaneous reference electrode. When needle biopsy revealed nondiagnostic necrotic material in the lesion, a reproducible electric potential difference usually could be demonstrated between the lesion and surrounding lung tissue. However, the electric potential of individual lesions varied from electropositive to zero to electronegative in relation to the surrounding tissue. Moreover, the electric potential of a lesion did not correlate with its histopathologic appearance. The reproducible electro-

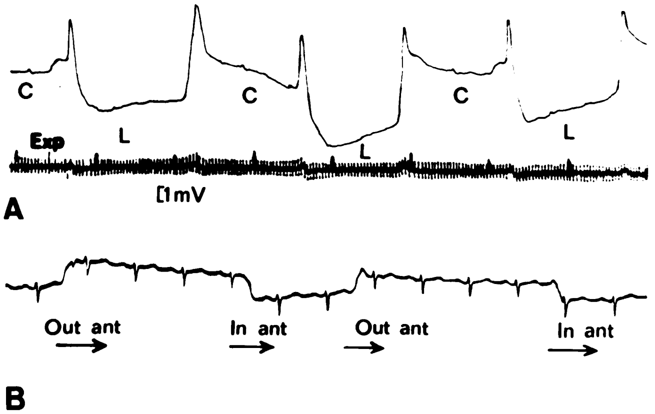

Fig. 1.—Electrical potentials in human lung tumors. **A**, Electropositive complexes (C) in squamous cell carcinoma in relation to surrounding lung (L) in 74-year-old man. Exp = exposure markings at cineradiography for correlation of position of electrode tip and tracing of electric potential. **B**, Electronegative complexes in metastatic melanosarcoma in right upper lobe of 57-year-old woman. "In ant" signifies electrode entering tumor surface; "out ant," electrode leaving tumor surface. (Reprinted from [2].)

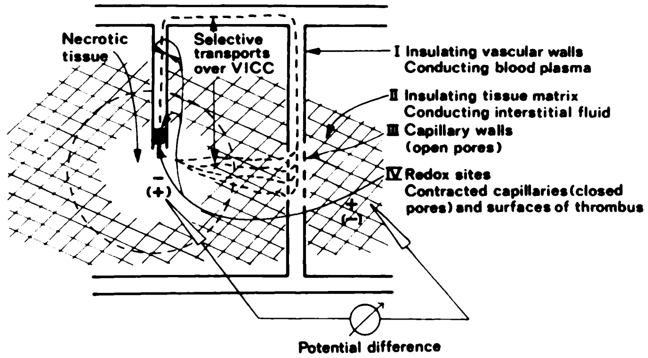
Necrotic tissue
Selective transports over VICC
I Insulating vascular walls
Conducting blood plasma
II Insulating tissue matrix
Conducting interstitial fluid
III Capillary walls
(open pores)
IV Redox sites
Contracted capillaries (closed pores) and surfaces of thrombus
–
(+)
+
(–)
Potential difference

Fig. 2.—Principle of activation and construction of vascular-interstitial closed electric circuit (VICC). Differences in metabolic activity of various tissues and organs as well as of any injured tissue in relation to noninjured tissue give rise to electrochemical potential differences. These are spontaneously leveled by ionic transports in VICC system because blood vessels function as relatively insulated conducting cables. Over capillaries, permeable for water and electrolytes, an electric junction exists to conducting interstitial tissue fluid, which closes circuit. Necessary electron transfers in circuit are localized to capillary membranes, which close their "leaking pores" in certain regions under influence of electric field. Endogenous currents of VICC system are predominantly responsible for development of corona structures, which represent a special case of healing of injured tissue. (Reprinted from [2].)

positive tissue profile of a necrotizing squamous cell carcinoma of the right lung in relation to the surrounding lung is shown in figure 1A. Figure 1B shows small, reproducible electronegative complexes of a necrotizing melanosarcoma.

In an attempt to explain the potential differences of lesions in relation to surrounding tissue, in vitro studies were performed of the electromechanical behavior of spontaneously degrading blood [2, pp. 69–78]. These studies may be summarized as follows:

Normal human blood was transferred under meticulous sterile conditions to a collodium bag suspended in 1 L of circulating Ringer solution. Then, pH electrodes were placed in the blood, and nonpolarizable Ag/AgCl electrodes in KCl bridges were immersed in the blood and the Ringer solution. A 2-cm layer of liquid paraffin was poured over the blood and the Ringer solution to prevent access of atmospheric oxygen and CO_2 to the blood.

The electric potential of the spontaneous hypoxic degradation of the blood was then followed in various experiments for 3–6 weeks. The results revealed that the hypoxic degradation of blood is a continuous, spontaneously oscillating process. Electropositive and electronegative phases alternate. The amplitudes of these phases attenuate as time passes.

Thus, a lesion that develops internal necrosis or contains degrading blood must show various time-related phases of shift of polarity and magnitude of potential differences. This concept of the fluctuating potential of injured tissue is essential for the electrogenous transports within the VICC system in the process of healing. No tissue can be expected to heal if supplied with only one type of ions. The fluctuating injury potential secures to the injury an ebb and flow, which both supplies and removes anionic and cationic material over the VICC system. Curiously enough, the injury itself seems thereby to deliver the necessary transport energy for its own healing. When the fluctuating energy potential has leveled out, the injury should be healed. The sequential development of the corona structures results from the fluctuations of the injury potential.

The driving electromotive force of the VICC system in tissue injury is twofold: (1) A so-called *diffusion potential* arises in the degrading tissue by the differential speeds of diffusion, convection, and recombination of liberated ions. Data already exist for the development of a change in diffusion potential during coagulation of blood. Thus, Jordan [4] found that the sequential steps in the process led to an overall potential change of as much as 1.5 V. (2) The hypoxia of the degrading tissue leads to a *redox potential difference* between the degrading tissue and surrounding well oxygenated tissue. The redox potential for O_2 is 0.82 V. The electromotive force for the activation of the VICC is therefore a sum of the continuously variable diffusion potentials of the degrading tissue and the redox potential differences between the hypoxic degrading tissue and the oxygenated surrounding noninjured tissue.

The electrochemical potential difference between a focus of necrosis or bleeding inside a lesion and the surrounding noninjured tissue resembles the conditions of an ordinary flashlight battery. To get an effect out of such a system, it is necessary to create a closed circuit between the two poles. In vivo, this circuit is created by the VICC.

Construction of the VICC System

Electric resistivity (a material constant) of the walls of arteries and veins was found in several ways to be at least 150–200 times higher than that of the plasma, the conductive medium of blood. To the blood vessels therefore can be ascribed a newly appreciated and important function: They are capable of serving as electrically conducting, relatively

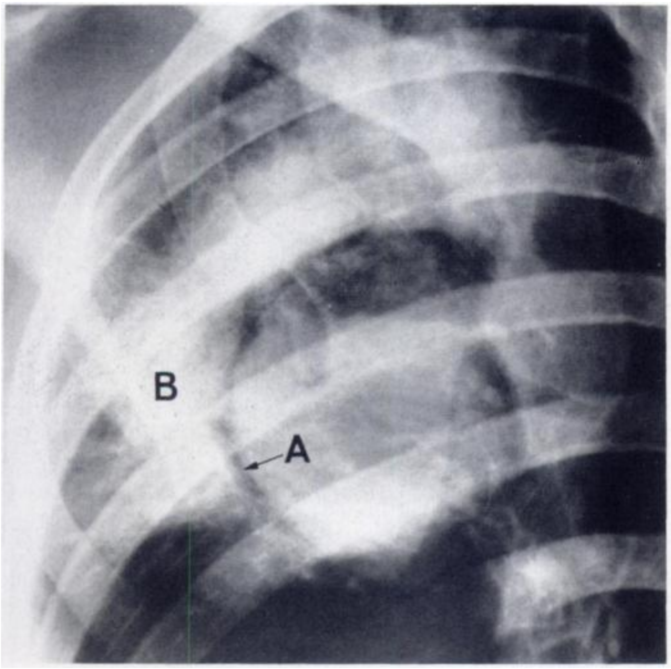

3

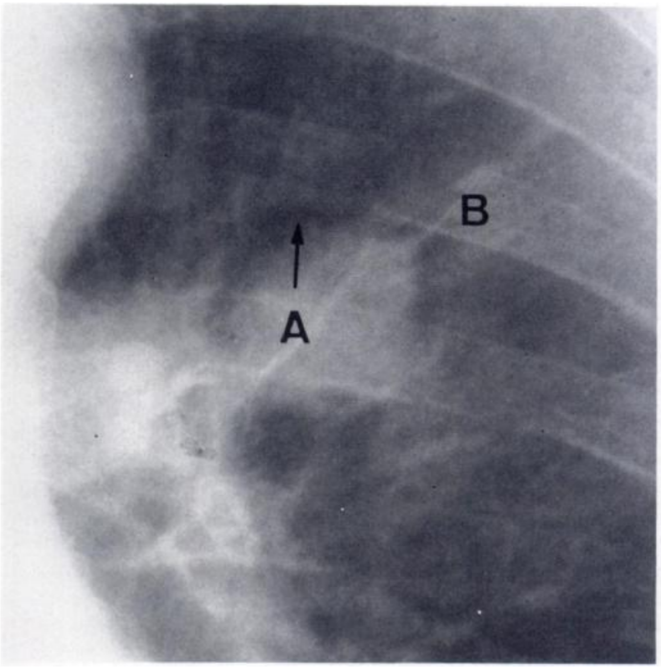

4

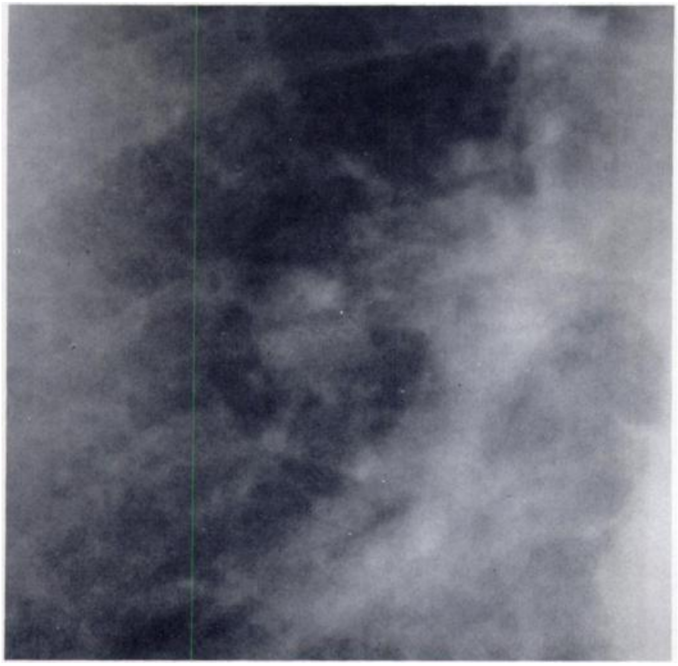

5

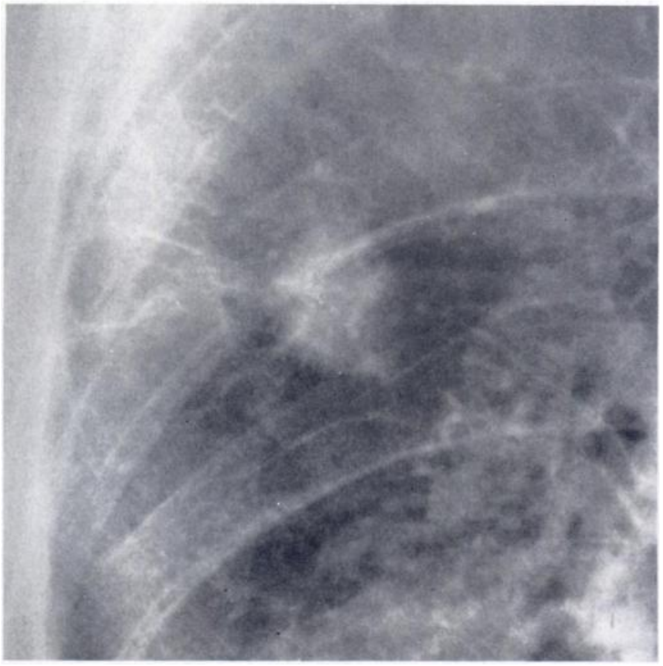

6

Fig. 3.—Squamous cell carcinoma in right upper lobe surrounded by 3–15-mm-wide radiolucent "A" zone (A) separating tumor from superolateral, 2–3-cm-wide radiopaque "B" zone (B). (Reprinted from [2].)

Fig. 4.—Poorly differentiated small-cell carcinoma surrounded by 5-mm-wide "A" zone (A). "B" zone (B) is seen as irregular infiltration lateral to tumor. B zone is always separated from tumor surface by A zone. (Reprinted from [2].)

Fig. 5.—Hamartoma in right lung surrounded by 5–10-mm-wide A zone. (Reprinted from [2].)

Fig. 6.—Silicotic granuloma surrounded by 1–2-cm-wide A zone. Edge of tumor is serrated, and irregular radiating structures extend to pleura. (Reprinted from [2].)

insulated cables. These cables connect injured with noninjured tissue (fig. 2) at the level of the capillaries, where an electric junction exists over the capillary membranes and between the endothelial cells to the interstitial fluid. This fluid, as conductive as plasma, can be regarded as the "internal" communication of our "biologic battery." The differences of electric potential between the injured and noninjured tissue regions can now be leveled by ionic transports over the VICC

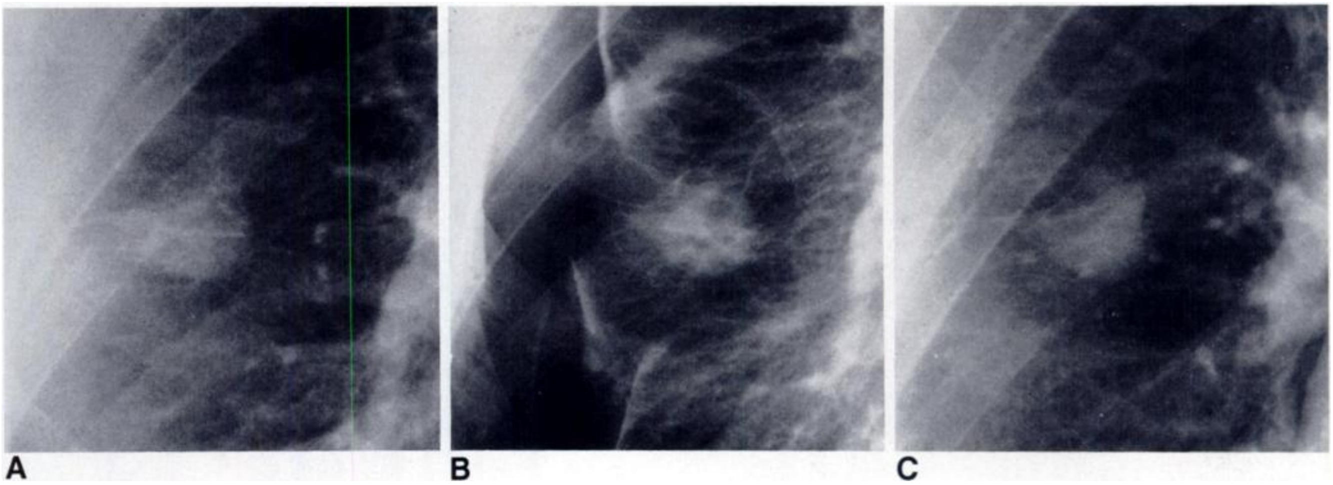

Fig. 7.—**A**, Tuberculous granuloma surrounded by A zone and granular radiating structures. **B**, 2 years later, pneumothorax was induced during needle biopsy. Note persistent A zone despite partial collapse of lung. **C**, After 2 more years, radiolucent A zone is even more apparent when lung is normally expanded. (Reprinted from [2].)

system. This new circulatory system meets the need of tissues for selective electrogenic mass transports. The construction of the VICC is, however, considerably more complicated than appears from this description. For instance, it contains identifiable switching mechanisms and necessary electrode-equivalent sites for electron transfer at the level of the capillaries. Information on these issues is given in the original description [2, pp. 134–151].

The activation of the VICC by tissue necrosis and/or degrading blood in cancers, benign tumors, or granuloma is likely to be the major common factor for the development of corona structures. These radiologically visible structural elements can be produced experimentally by in vivo activations of the VICC. Many histologic and chemical modifications in tissues also can be identified and tied to activation of the VICC. From a general biologic standpoint, it is therefore important to study the corona complex: it represents a specific case of injury reaction and can unveil essential events in the process of healing.

The Radiologic Appearance of the Corona Structures

The corona structures vary widely in extent of development and time of their appearance. To quantitate them radiographically is as difficult as to quantitate emphysema radiographically. Examples will be given to illustrate their development largely as a result of catabolic activation of the VICC system.

The A Zone

The A zone is characterized by a "halo" or radiolucent area around all or a portion of a radiopaque mass. Its width ranges from 2 mm to 8 cm and may vary in different parts of the zone. The inner border of the A zone is limited by the surface of the tumor. The outer border of the A zone may be well defined against a denser B zone. In figure 3, a squamous cell carcinoma of the right upper lobe is surrounded by a 3-mm-wide A zone and a B zone about 2–3 cm wide. The outer border of the A zone may be ill defined, as is seen around the small-cell carcinoma shown in figure 4.

The A zone may also appear around benign tumors. This is illustrated in figure 5, where a 5–10-mm-wide A zone surrounds a hamartoma.

Granulomas may also show A zones. Thus, the silicotic granuloma shown in figure 6 is surrounded by an A zone 1–2 cm wide. When an A zone extends over time, a more permanent A zone develops as perifocal emphysema. An example may be seen around the tuberculous granuloma of figure 7A, which was followed radiographically and by needle biopsies over 8 years. Initially it showed a faint A zone and radiating "granular" structures in the nearby lung parenchyma as well as an arcuate displacement of a vessel cranial to the lesion. A pneumothorax developed in connection with a needle biopsy of the lesion. Despite the partial collapse of the lung, the A zone persisted around the tuberculoma (fig. 7B). Two years later, the reexpanded lung showed a well developed A zone.

The B Zone

This structural element represents a region of increased radiopacity peripheral to the A zone. Its opacity is greater not only than that of the A zone but also than that of normal lung (figs. 3 and 4). For peripherally situated lesions, the B zone often extends from the periphery of the A zone to the pleura. When a small amount of air is injected into the pleural space, the B zone disappears completely, a characteristic finding (fig. 8).

Radiating Structures

These linear structures emerge from the surface of the lesion. They may be short and thin and give the surface of the lesion a "hairy" appearance. They may also be coarse and

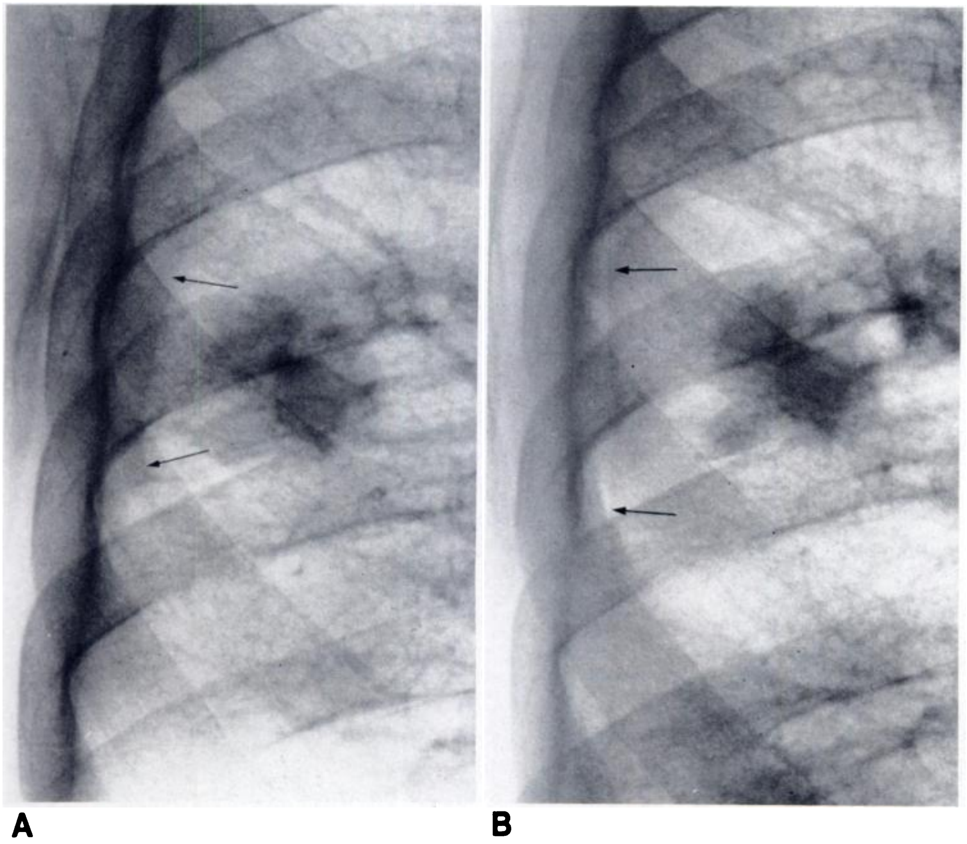

Fig. 8.—Squamous cell carcinoma. **A**, B zone (*arrows*) adjacent to pleura; A zone between tumor and B zone. **B**, B zone disappears when air is injected into pleural space. (*Arrows* in **B** indicate visceral pleura.) (Reprinted from [2].)

sometimes extend several centimeters into the lung parenchyma (fig. 9). Characteristically, the surface of the associated lesion is irregular. The radiating structures depart at approximately right angles to this surface, a finding particularly apparent in lesions in the vicinity of the pleura (fig. 10). In this example, a metastatic adenocarcinoma shows fine radiating structures more or less perpendicular to the surface of the tumor. If these structures represented lymphatic growth, they should have taken a convergent course toward the hilum. The radiating structures grow more or less straight through the various tissue elements of the lung and are radiographically apparent by summation as continuous "lines." A lesion with a smooth surface does not show any radiating structures. Histologically the radiating structures consist mainly of fibrous material. Near a malignant tumor they may enclose islands of cancer cells and vessels.

Arches and Arcades

These structures develop at the interface between an A and a B zone and have been observed only in the presence of radiating structures. The appearance of the arches in the radiographs varies with the projection. The A/B zone interface in figure 11 presents small arches, each 1–2 mm in diameter, in a left anterior oblique projection. As a group, these arches form a row or arcade.

Another example of small arches forming an arcade is shown in figure 12. This adenocarcinoma of the lung showed central necrosis, small hairlike radiating structures, lamellae, and a radiolucent A zone. The faint B zone is evident peripheral to the 1–2-cm-wide A zone. Close inspection of the superolateral interface between the A and B zones suggests a 2-cm-long arcade consisting of 1–2-mm-wide arches.

To facilitate understanding of how the VICC system functions, I interrupt the description of the remaining corona structures in order to examine the intregrated action of the electrical forces of the system with molecular (chemical concentration) and volume-pressure forces in the development of the structural elements so far described.

Mechanism of Development of the A and B Zones, Radiating Structures, and Arches and Arcades

These structures were the first radiographically observed structural elements of the corona complex. They were produced experimentally in vitro and in vivo in dogs on the basis of structuring of material within a closed electric circuit. The underlying mechanism for their development is shown by the in vitro experiment illustrated in figure 13.

A small aluminum ball with small, irregular protrusions on its surface was connected to a cable and glued to the bottom of a glass jar. Thin aluminum foil was glued to the inner wall of the jar and also connected to a second cable. Liquid paraffin was poured up to the equator of the ball. After short-circuiting of the two cables (to exclude any electric field gradient in the liquid paraffin), semolina grains (particles of dielectric, "noncharged" material) were scattered as evenly as possible over

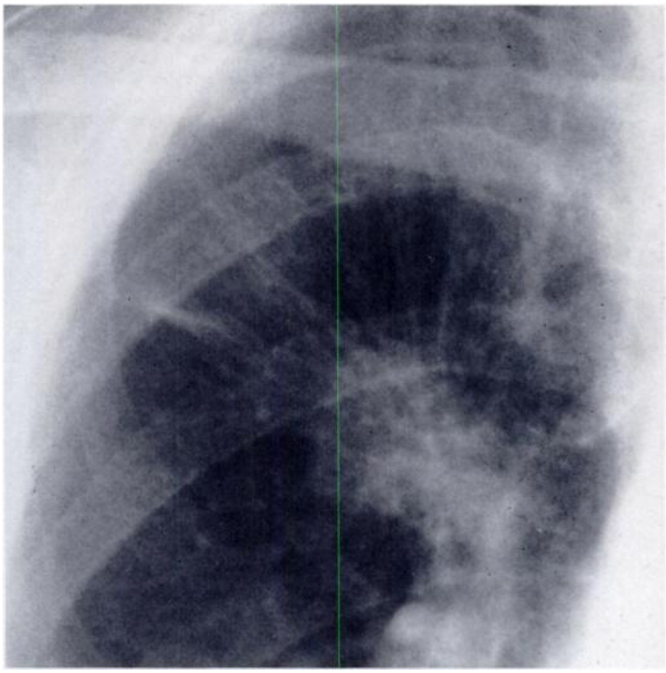

9

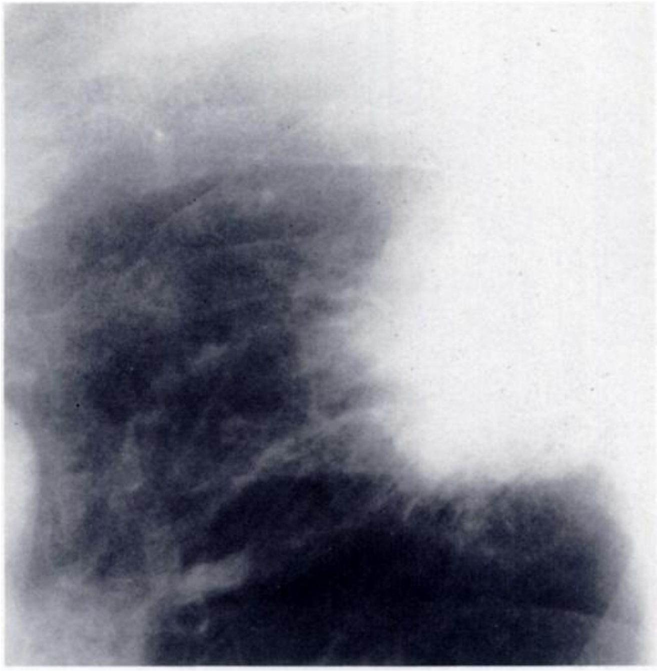

10

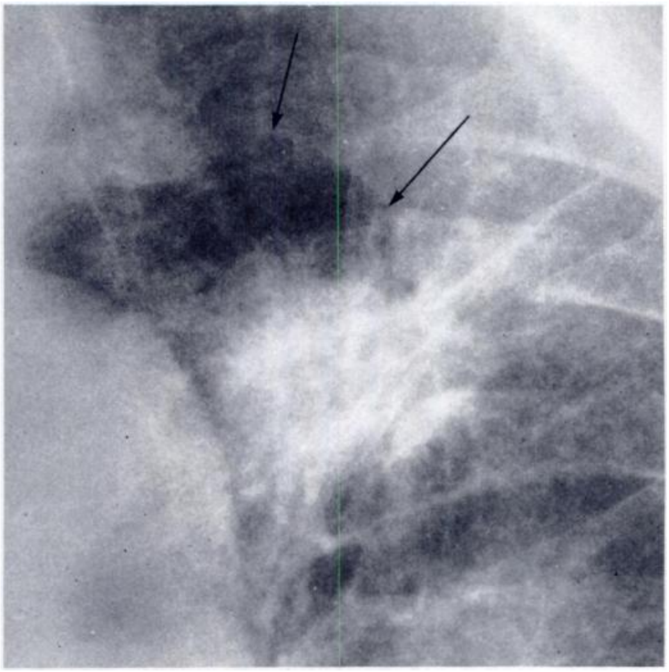

11

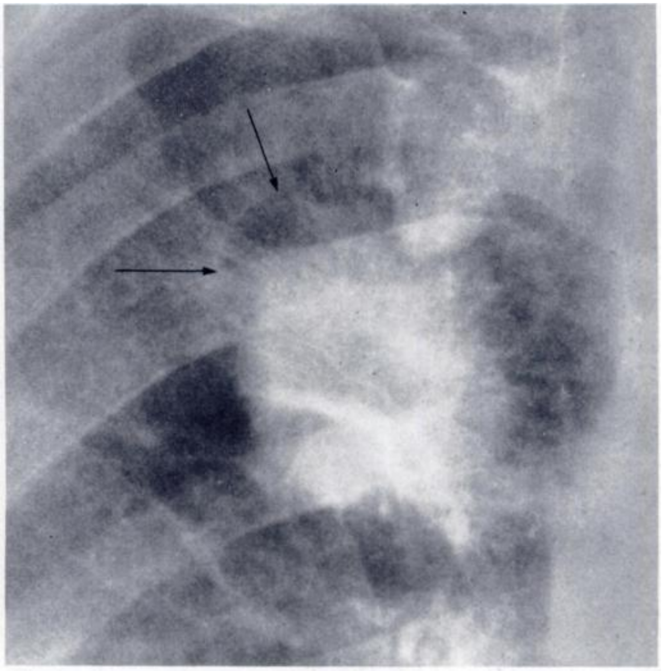

12

Fig. 9.—Metastatic breast carcinoma with numerous long, coarse, radiating structures perpendicular to surface of tumor. No preformed channels in lung, such as lymphatics, have this orientation. (Reprinted from [2].)

Fig. 10.—Metastatic adenocarcinoma adjacent to pleura. Fine structures radiate more or less perpendicularly to surface of tumor. No preformed channels in the lung have such a course. (Reprinted from [2].)

Fig. 11.—Squamous cell carcinoma of left upper lobe. Small arches form an arcade (*arrows*) at interface between A and B zones. (Reprinted from [2].)

Fig. 12.—Adenocarcinoma with internal necrosis, hairlike radiating structures, a radiolucent A zone, and small arches forming an arcade (*arrows*). (Reprinted from [2].)

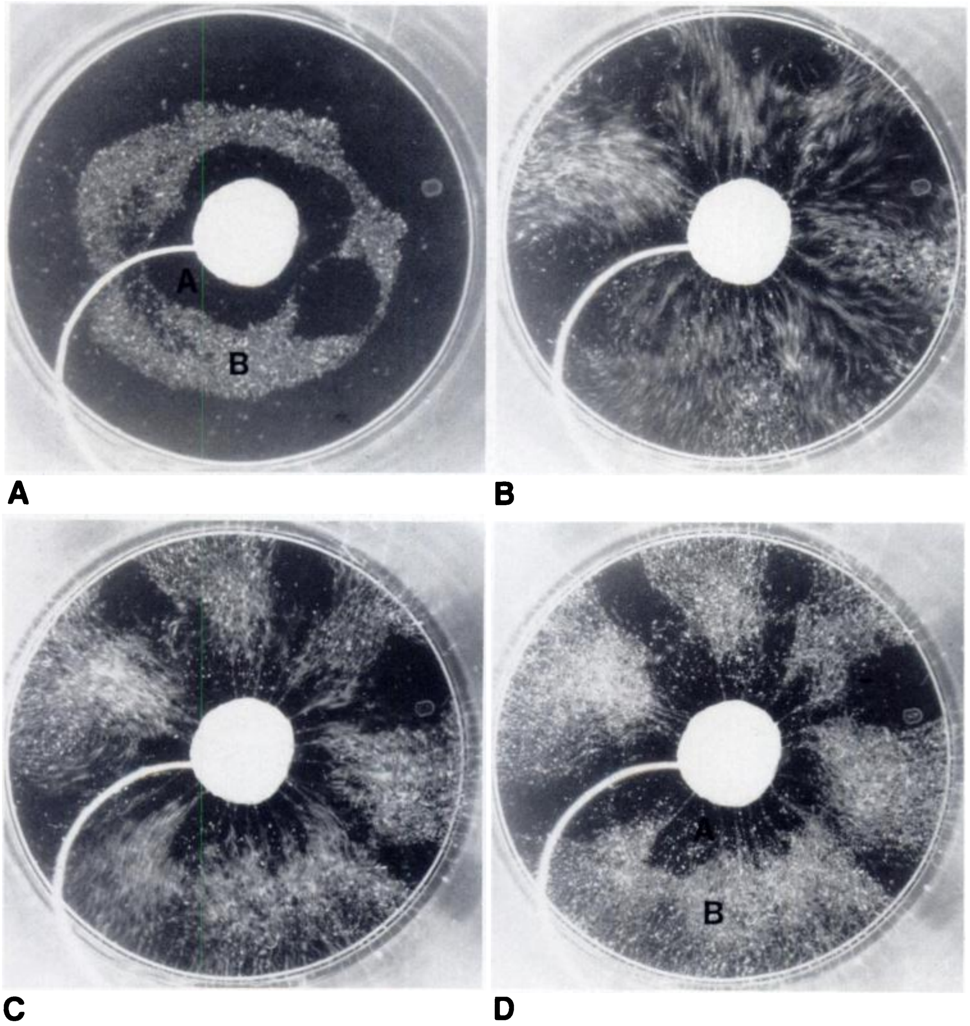

Fig. 13.—In vitro production of A and B zones, radiating structures, and small arches forming an arcade. An aluminum ball with small, irregular protrusions on its surface was glued to inside bottom of jar (seen from above; transilluminated from below). Ball and aluminum foil lining jar were each connected by cables to DC potential generator. Liquid paraffin was poured into jar up to equator of ball. **A**, Short-circuiting of terminals. Dielectric semolina grains sifted onto the liquid surface are structured as A and B zones between aluminum terminals. **B**, 5-sec exposure during application of 1.5 kV potential. Semolina grains have started to move in electric field. Ten seconds later (**C**), grains are arranged in radiating structures around ball with preference for surface protrusions. **D**, 10 sec after **C**, grain movements have stopped, showing radiating structures, a halo or A zone, a higher concentration of grains or B zone outside halo, and small arches forming an arcade at interface between A and B zones. Note that two arches are supported at each junction by one radiating structure. (Reprinted from [2].)

the surface of the liquid. As a collection, they contracted spontaneously on the surface of the liquid by their internal molecular concentration forces, forming what may be regarded as an A and a B zone (fig. 13A). When an electric potential (1.5 kV) was applied between the ball and the periphery, the grains started to move, as shown by the motion blur during a 5-sec photographic time exposure (fig. 13B). Competition between electric field and concentration forces then produced a new structuring of the grains (fig. 13C). A new equilibrium eventually ensued (fig. 13D). Furthermore, the phenomenon of electrical edge enhancement caused radiating structures to develop opposite the protrusions of the surface of the ball. At the interface between the A and B zones (fig. 13D), small arches can be seen to form an arcade. Each radiating structure supports the junction of two adjoining arches. This in vitro experiment was performed to illustrate the interaction between electrostatic and molecular forces. In vivo, ionic and nonionic (dielectrophoretic) transports can take place in tissue fluids at low voltages. The analogous structuring described for lung masses has its origin in a similar balance of electrostatic and molecular forces.

Electric transport of nonionic material is called dielectrophoresis. The electric transport of water (a dielectric material) is known as electroosmosis. This process has several mechanisms [2, p. 82], but the net transport can be illustrated as follows:

A U-shaped glass tube is partly packed with cotton and partly filled with water (fig. 14). When a potential difference is applied between two platinum electrodes, water will move from the electropositive to the electronegative side. This electroosmotic transport evidently is balanced by the hydrostatic pressure difference between the two fluid levels. Prerequisites for this water transport are narrow "capillaries" provided with fixed surface charges and a closed electric circuit powered over the electrodes. The packed cotton, which forms "capillaries" among the fibers, contains a surplus of fixed electronegative charges. Under these circumstances, water moves from the electropositive to the electronegative side of the system. In vivo, the interstitial spaces of any tissue will behave like the cotton because the surfaces of all body cells are lined with a surplus of fixed electronegative charges [5]. Electroosmotic transports of water producing A and B zones occur regularly in vivo in patients undergoing percutaneous electrochemical treatment of cancer [2, p. 302].

Such an in vivo experiment is illustrated in figure 15. The positions of a platinum anode (+) and a platinum cathode (−) before treatment are shown in figure 15A. After delivery of 250 C at 10 V electrode potential, cavities were formed by gas production around the electrodes (anodic O_2 and Cl_2 and cathodic H_2). A radiopaque halo (B zone) is seen in the lung parenchyma around the former site of the cathode. The B zone is caused by excessive electroosmotic inflow of tissue water (fig. 15B). The local edema spontaneously resorbed a few hours after the conclusion of the 2-hr treatment.

Consider now the situation of a mass in the periphery of the lung (fig. 16). The mass presents an electropositive phase (i.e., an early phase of internal necrosis) in relation to surrounding lung tissue. Consider also that some of the interlobular spaces between the mass and the pleura are mechanically blocked by the tumor. On activation of the VICC system, a closed-circuit electroosmotic transport of water will take place from the tumor, leaving a hydropenic radiolucent zone (A zone) between the tumor and the hydropic radiopaque zone (B zone), which contains excess tissue water. The position of the interface between the zones will then be determined by the equilibrium between the electroosmotic force and the counteracting elevation of the turgor pressure by the tissue edema resulting from the blocked interlobular spaces.

Whenever a tumor has surface protrusions, radiating structures will develop by edge enhancement of the electric field. Dielectric material in the tissue fluid will arrange itself along "field lines" and subsequently be transformed into scar tissue. At the interface between the A and B zones, a small arch bridges each adjacent pair of radiating structures, which also serve to stabilize the arches. The convexity of these arches is always directed away from the tumor.

I now return to the description of the corona structures, keeping in mind that the VICC system and molecular- and volume-pressure forces all interact in the development of the remaining eight structures. Additional integrated mechanisms also are involved.

Lamellae

Linear structures sometimes appear to cross a lesion. Figure 17A shows such a lesion with at least two "lines." When the patient is examined in various projections, it is usually possible to show that these lines are superimposed linear structures in the surrounding tissue (fig. 17B).

The development of the linear structures is conceived to take place in three stages, as illustrated in figure 18. A cancer (stage 0) undergoes internal necrosis and develops radiating structures, as described previously (stage 1). The necrotic content may evacuate into a bronchus and be replaced by air (stage 2). On reocclusion of the bronchus (e.g., by tumor growth), air is resorbed, leading to collapse of part of the tumor surface. Displacement of previously developed radiating structures will then take place, leading to the radiographic appearance of linear structures (stage 3), which in certain projections appear to cross the tumor. These modified radiating structures are called lamellae.

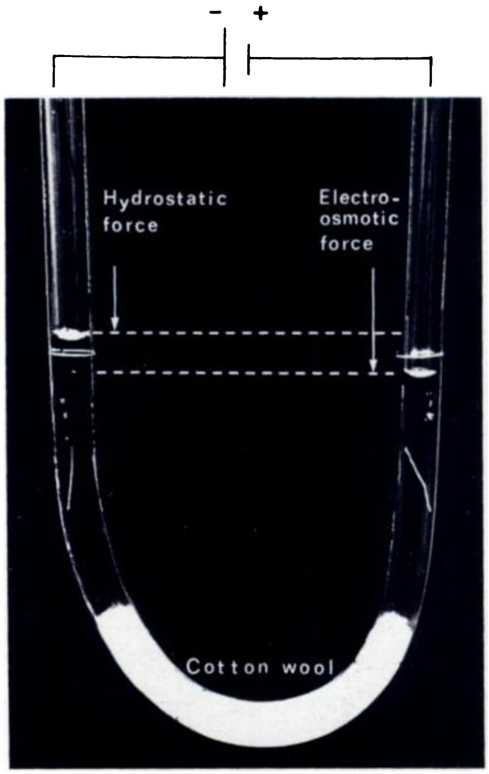

Fig. 14.—Electric transport of water. Cotton wool is packed into lower part of U-shaped glass tube, which is partly filled with water. Two clean platinum electrodes are immersed. When an electric potential difference is applied between electrodes, water moves in "capillaries" of cotton fibers from electropositive to electronegative side of system, creating equilibrium between opposing electroosmotic and hydrostatic forces. (Reprinted from [2].)

Circumferential Structures

In the lung, vessels often can be seen to take a circumferential course at a distance from a lesion, peripheral to an A zone. Circular displacement of structures can be detected readily by computed tomography (CT). Thus, in figure 19A the radiolucent A zone is barely recognizable in the region medial to a large squamous cell carcinoma. In the corresponding CT scan (fig.19B), circular displacement of vascular structures medial to an A zone is easily seen.

By CT it is possible to demonstrate a lower attenuation for x-rays in the lung parenchyma of the A zone inside the displaced vessels as compared with the attenuation in surrounding lung parenchyma. A plain radiograph of a pulmonary

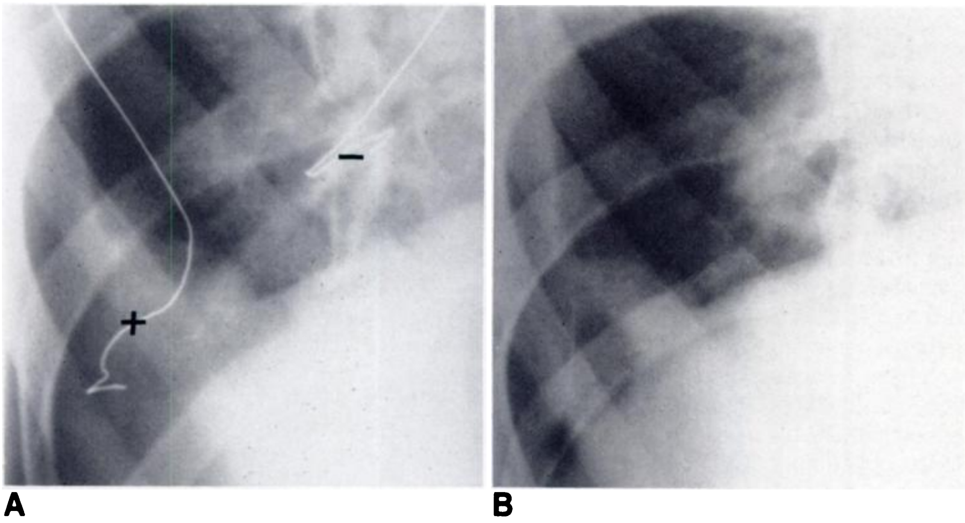

Fig. 15.—Metastatic fibroliposarcoma of right lung. **A**, Anode (+) in tumor and cathode (−) in lung parenchyma before percutaneous electrochemical treatment with 250 C of direct current at 10 V. **B**, Immediately after treatment, cavities are present at site of each electrode; a gas cavity is seen in tumor, and electroosmotic edema surrounds cavity at former site of cathode. (Reprinted from [2].)

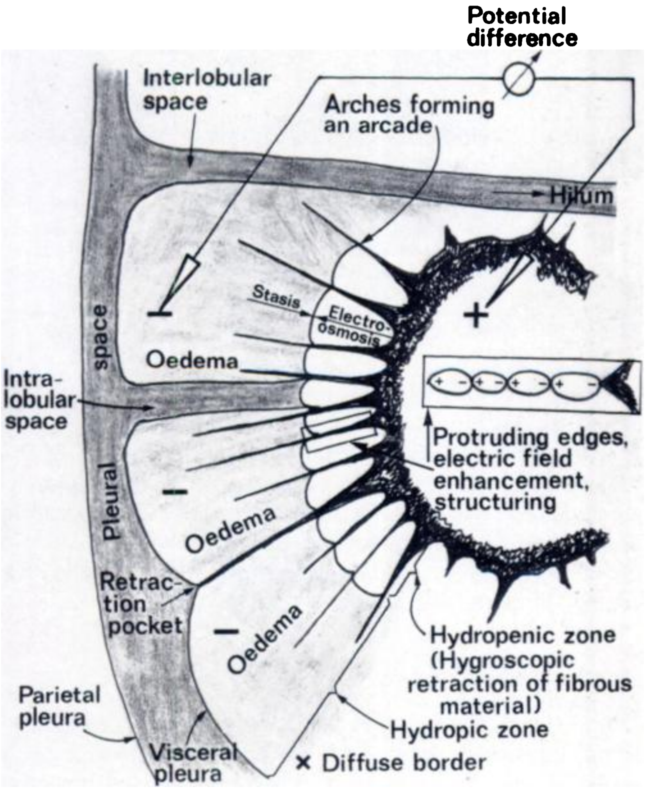

Fig. 16.—Diagrammatic representation of water distribution around tumor. Tumor that develops internal necrosis will liberate catabolic energy, activating VICC channels between tumor and surrounding tissue. Radiating structures follow electrical field lines and are therefore unrelated to preformed tissue channels. Tumor produces stasis of tissue fluid by blocking of interlobular channels. This fluid is moved by electroosmosis from electropositive tumor surface toward electronegative lung tissue, which leads to development of radiolucent hydropenic A zone and a radiopaque hydropic B zone. Small arches will develop at interface between zones. (Reprinted from [2].)

metastasis from a malignant melanoma does not clearly demonstrate any perifocal radiolucency (fig. 20A). The corresponding CT scan, however, shows the circular displacement of vessels and an A zone of 24 H lower mean attenuation than the mean attenuation of the surrounding lung parenchyma (fig. 20B).

Narrowing of Vessels

Small vascular branches from a circularly displaced vessel often show a pronounced tapering in their caliber in the A zone. Such tapering of vessels is seen around a poorly differentiated squamous cell carcinoma (fig. 21). One vessel behind the tumor is probably circularly displaced. A small vessel running perpendicularly toward the A zone seems to be blocked. Such vascular obstruction can also be seen around granulomas and benign tumors. Around the hamartoma shown in figure 22, the A zone is 1–5 mm wide. A branch vessel appears to be blocked at the border of the A zone. Histologically, narrowing of vessels was found to be caused by thrombosis of small vessels [2, p. 176].

Perifocal Emphysema

Emphysema developing around a polarizing process may also contribute to the lowering of the attenuation values within an A zone. Emphysema is properly defined as a loss of structured tissue components. In vivo microscopy of the mesentery of dogs revealed that multiple segmental contractions develop acutely in small vessels when they are exposed to electric fields [2, pp. 135–247]. Microthromboses develop in the anodic field. Chronic obstruction of small vessels can be expected to lead to permanent regressive changes of the lung parenchyma in the A zone and consequently to the development of true perifocal emphysema. The chronic process of the tuberculous granuloma shown in figure 7 may have

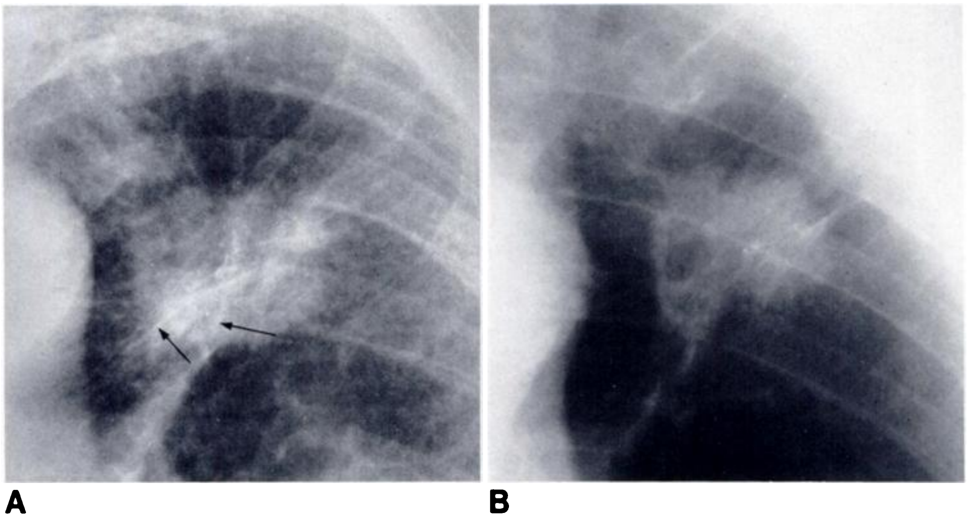

Fig. 17.—Moderately well differentiated squamous cell cavitary carcinoma, presenting lamellae. These linear opacities appear to cross each other over tumor in posteroanterior projection (**A**, *arrows*). In slight left posterior oblique projection (**B**), lamellae are projected at surface of tumor. (Reprinted from [2].)

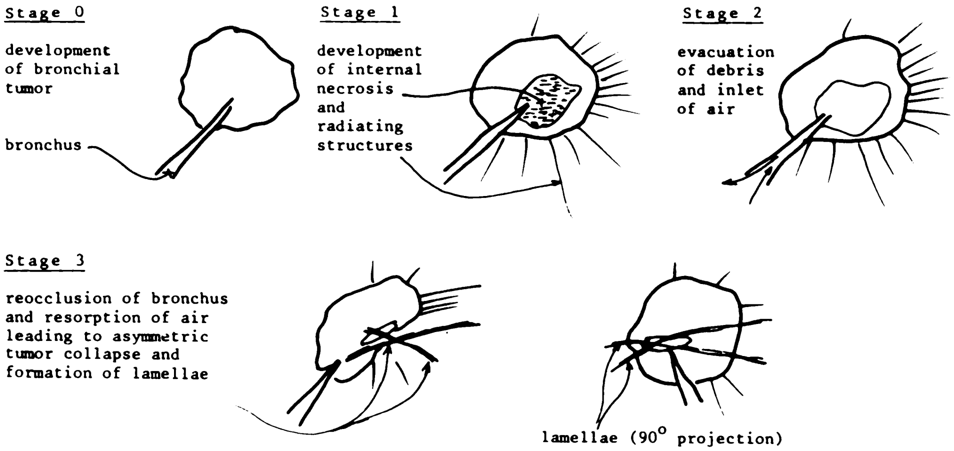
Stage 0
development of bronchial tumor
bronchus
Stage 1
development of internal necrosis and radiating structures
Stage 2
evacuation of debris and inlet of air
Stage 3
reocclusion of bronchus and resorption of air leading to asymmetric tumor collapse and formation of lamellae
lamellae (90° projection)

Fig. 18.—Proposed principle of formation of lamellae. *Stage 0*: Pulmonary mass develops around bronchus. *Stage 1*: Eccentric local necrosis develops in tumor, and tissue degradation leads to development of radiating fibrous structures perpendicular to tumor surface. *Stage 2*: Necrotic debris leaves tumor via bronchus and is replaced by air. *Stage 3*: Bronchus becomes blocked, leading to resorption of air in tumor cavity. Asymmetric collapse of tumor tissue will produce local conglomeration of radiating structures in surrounding lung tissue. Lamellae developed in this way may appear to cross tumor in certain projections. (Reprinted from [2].)

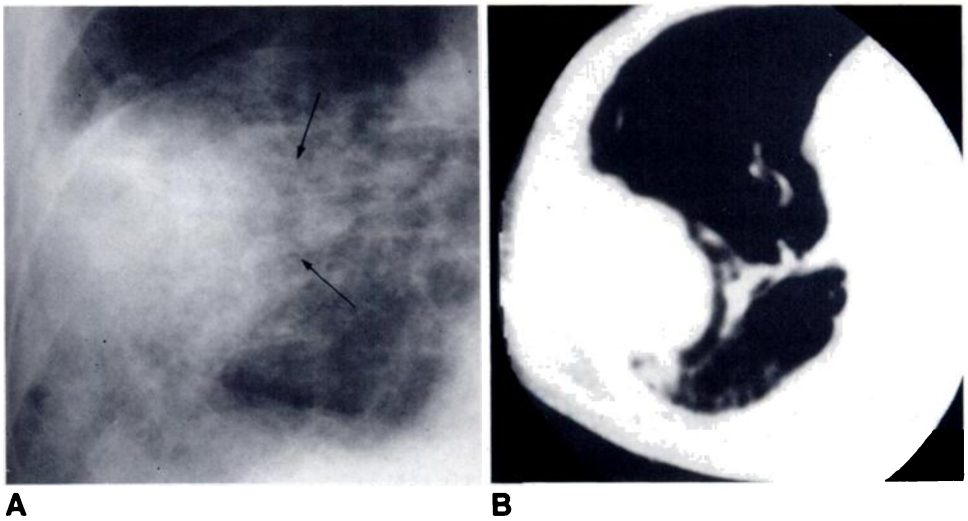

Fig. 19.—Circular displacement of vessels around squamous cell carcinoma of right lower lobe. **A**, Barely visible radiolucent zone medial to tumor (*arrows*). **B**, Transverse CT scan at level of center of tumor. Large pulmonary vessels medial to tumor seem to avoid its surface. Radiolucent zone here appears clearly interposed between vessels and mass. (Reprinted from [2].)

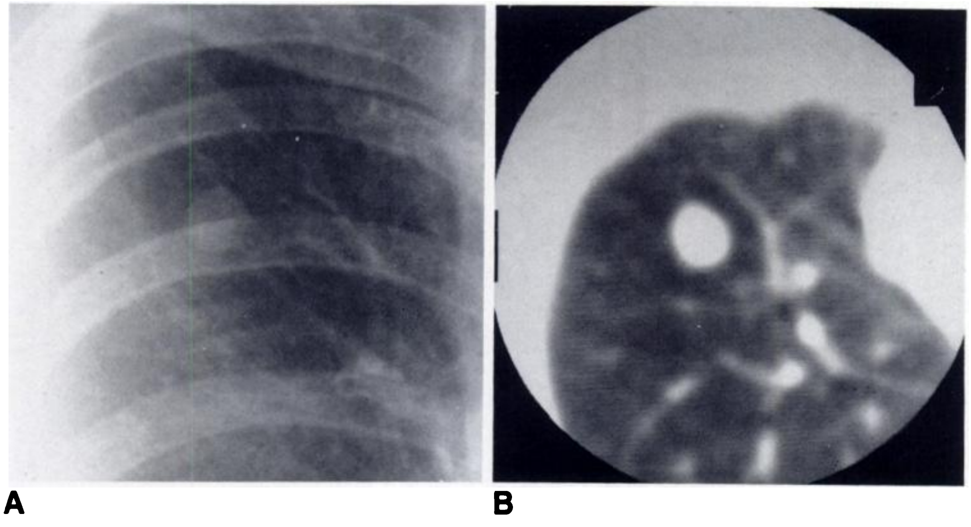

Fig. 20.—Metastasis from malignant melanoma. In radiograph (**A**), only a faint A zone is suggested. In CT scan (**B**), vessels are circularly displaced around A zone of lower mean attenuation (24 H) than surrounding lung parenchyma. (Reprinted from [2].)

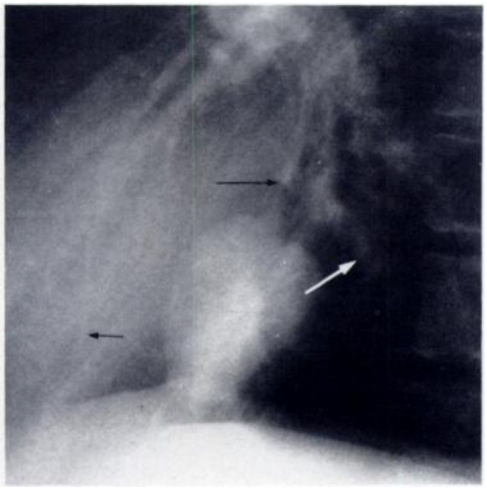

21

Fig. 21.—Poorly differentiated squamous cell carcinoma in right lower lobe (lateral view). Lung tissue around tumor shows absence of vessels, while visible vessels at edge of A zone are narrow (*short black arrow*), displaced (*white arrow*), or even blocked (*long black arrow*). (Reprinted from [2].)

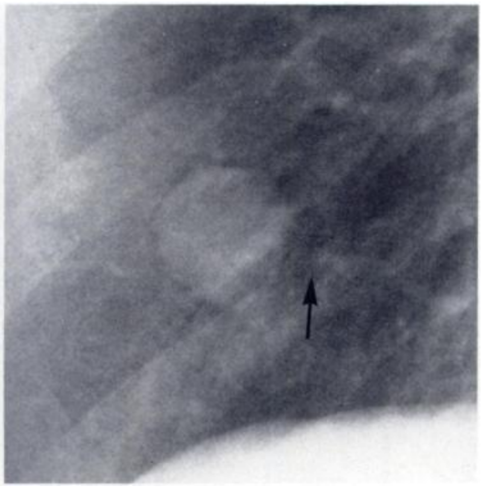

22

Fig. 22.—Hamartoma in right lung with narrow A zone surrounding tumor. A pulmonary vessel (*arrow*) appears not to transverse A zone. (Reprinted from [2].)

developed its A zone in this manner. Like an emphysematous bulla, this perifocal emphysema did not collapse even in the presence of a fairly large pneumothorax. For the radiologic identification of perifocal emphysema, regressive tissue changes of this sort must be demonstrated.

Perifocal Edema

This condition is a common finding at certain stages of development of malignancies and inflammatory lesions in the lung as well as in other organs (e.g., brain and breast). It is characterized by absence of a sharp borderline between the lesion and the surrounding tissue. Around breast cancers the perifocal opacity has been demonstrated both qualitatively and quantitatively to be caused predominantly by tissue water [2, pp. 216–231]. When measured, the electric potential in such cancers was electronegative in relation to surrounding tissue, a situation in which tissue water will move electroosmotically from surrounding normal tissue toward the tumor and its periphery. This corresponds to the accumulation of tissue water induced around the cathode shown in figure 15B. The turgor pressure will then increase in the previously developed A zone around the cancer and enhance the circular displacement of vessels (and other tissue elements) and contribute to narrowing of vessels by compression. In fact, in a dog's lung, an applied electronegative field led to complete suspension of the circulation in pencilwide vessels due to inflow of tissue water [2, p. 193]. The development of perifocal edema during an electronegative phase of a lesion and of an A zone during an electropositive phase reflects the time-dependent variations of polarity of the fluctuating potential of the degrading tissue in the tumor.

Interlobular Edema

Interlobular edema is characterized by visible interlobular spaces that are wider at their pleural than at their proximal extensions in the lung. This appearance makes it possible to

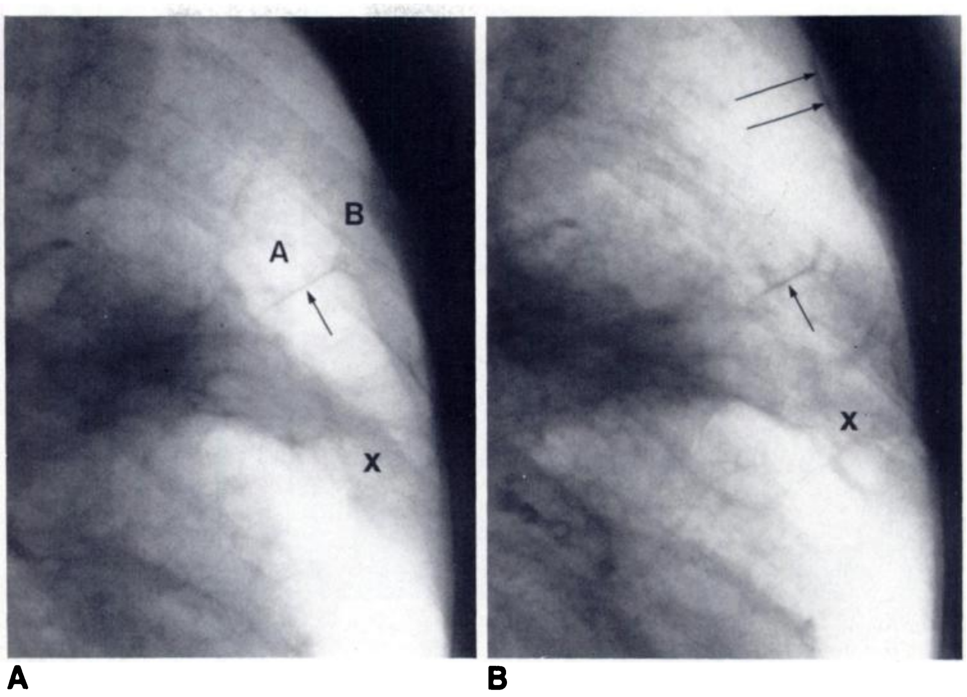

Fig. 23.—Carcinoma in right upper lobe (lateral view). **A**, Tumor produces atelectasis (X). Water is moved from tumor surface, leading to development of hydropenic A zone (A) and hydropic B zone (B). At their interface, electroosmotic pressure and counteracting edema balance each other. Linear structure (*single arrow*) represents fluid-filled interlobular space. **B**, Fluid in interlobular space is retained by capillary force even after injection of small amount of air (*two arrows*) into pleural space. B-zone water has disappeared into opened pleural space, but atelectasis remains. (Reprinted from [2].)

distinguish these "radiating" structures from the fibrous radiating structures previously described.

The interlobular edema may at a first glance seem indistinguishable from the so-called Kerley lines that develop as a result of acute or chronic stasis in the pulmonary circulation. The actual lines, however, characteristically result from several locally interacting factors within the mechanisms behind the corona complex. They develop during the electropositive phase of a degrading process. Water is transported electroosmotically from the lesion toward the pleura, producing a hydropenic A zone and a hydropic B zone (fig. 23A). From the B zone in this example, an inward tapered linear structure can also be seen. This structure represents a fluid-filled widened interlobular space. When a minimal amount of air was injected into the pleural space, the B zone disappeared. The interlobular fluid collection is still present. Why has tissue water moved from the tumor to form the B zone while fluid remains in the interlobular space within the hydropenic A zone? The physical explanation is that the electroosmotic force is effective only when the "capillarity" of the interstitial spaces is characterized by narrow channels. The interlobular space is too wide for effective electroosmosis; instead, local turgor pressure by stasis is the dominant mechanism for focal edema. Hence, a fluid-filled widened interlobular space is seen within the hydropenic A zone as in figure 23A.

Fibrous Tissue

I again temporarily interrupt the description of the individual corona structures and turn to a remarkable effect of an activated VICC system: the production of fibrous tissue.

Transformation of normal tissue into fibrous scar tissue by direct current. When any tissue that can develop scar tissue is exposed to weak electric current for a sufficient period, fibrous tissue will develop. Current flowing from a smooth surface will lead to the development of a fibrous membrane parallel to the surface. Current flowing from protruding edges will lead to the development of linear fibrous structures. Their endogenous counterparts are the radiating fibrous structures. Part of the underlying mechanism was illustrated in figure 13, where the gross morphologic arrangement of radiating structures was shown to take place by the mechanism of electrical edge enhancement. In tissue, a multitude of modifications of cells also takes place under the influence of electric current. Here, I deal specifically with the development of fibrosis.

In vivo fibrous transformation of normal rat lung by unidirectional flow of direct current. Both lower lobes of a normal rat were resected. One control lobe was immediately fixed in formaldehyde whereas the other lobe was wrapped under nonsterile conditions in a thin polyethylene foil. Flat platinum electrodes were inserted into the open ends of this electrophoretic chamber. Soft-tissue radiographs were obtained of the specimen before and after electrophoretic treatment of the specimen (fig. 24). The current generator was constructed to operate either with constant current or constant electrode potential. The application of 10 μA of constant direct current required initially 0.8 V. Because of electroosmotic dehydration, daily application of a few drops of saline solution to the anodic electrode was necessary to keep the voltage below 2 V. The experiment was continued for 21 days. The specimen then showed lower cathodic (−) than anodic (+) density (fig. 24). Specimens treated in this way do not show bacteriologic decomposition, an effect interpreted as a bacteriostatic effect of the current.

After fixation in formaldehyde, the two specimens were sectioned and stained with hematoxylin-eosin and van Gieson stain. The control specimen showed normal lung tissue,

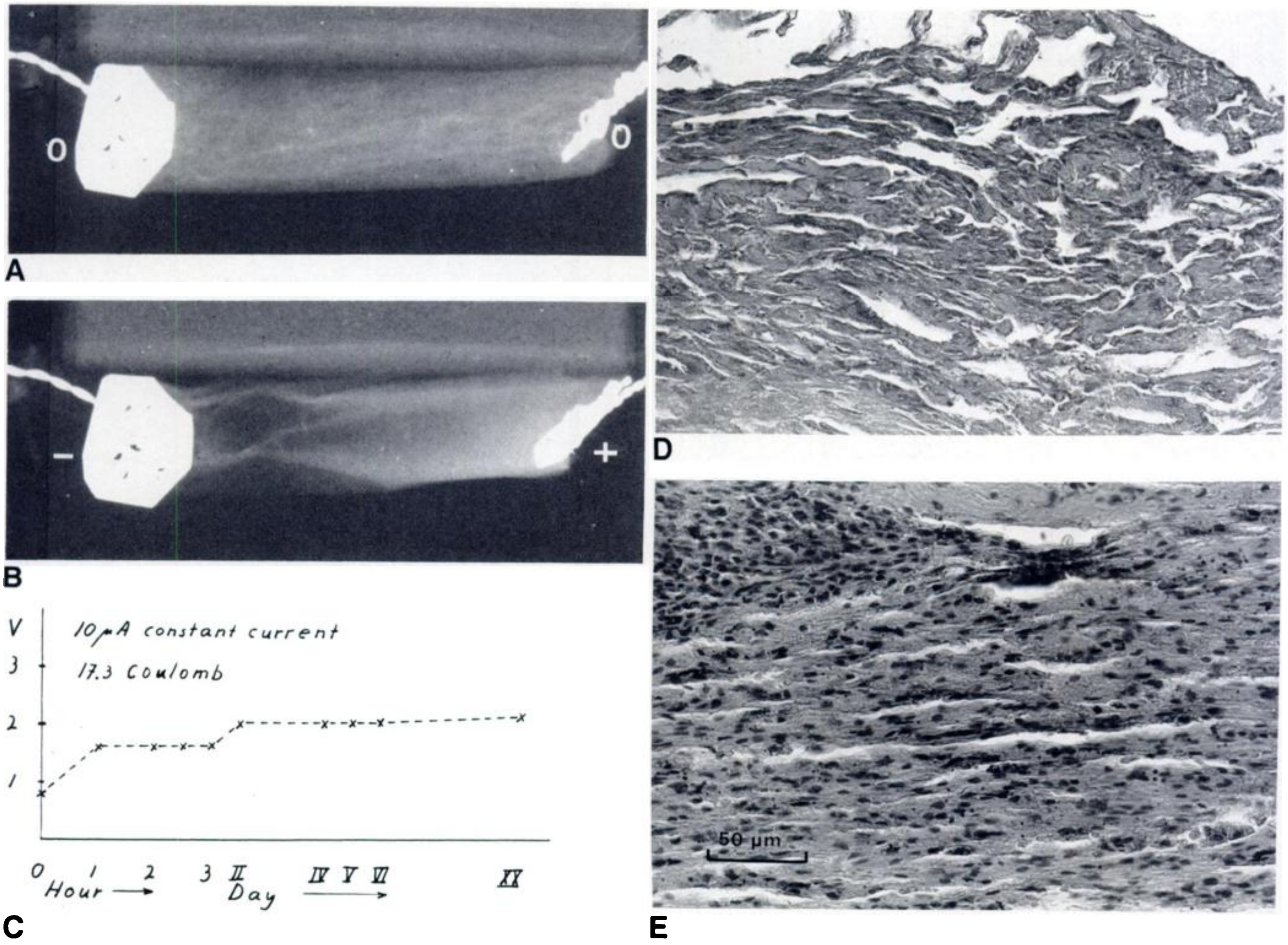

Fig. 24.—Induction of fibrosis in vitro. Right lower lobe of rat lung was wrapped in polyethylene foil to form electrophoretic chamber about 25 mm long with platinum electrodes at open ends. Soft-tissue radiographs before (**A**) and after (**B**) application of **C**, direct current (10 μA, 0.8–2 V) for 21 days. Cathodic (−) half is less radiopaque than the anodic (+) half. Histologic specimens: Cathodic part (**D**) contains fibrous tissue without any cell-like structures; anodic part (**E**) contains fibrous tissue and many fibroblastlike cells. (H and E stain.)

whereas extensive tissue and cell transformations were present throughout the electrophoretically treated "dead" lung lobe. In the cathodic (−) half of the treated specimen, very few cellular elements were preserved. The tissue was less dense than in the anodic (+) half. It contained birefringent tissue elements, as in collagenous fibrous tissue, and nowhere were any fibroblasts seen (fig. 24D). The anodic half of the specimen showed a compact fibrous tissue with many fibroblastlike cells of slightly varying size and shape (fig. 24E). These changes also were produced in later experiments at currents below 1 μA. The histologic staining of the specimens indicated that collagenous fibrous tissue was produced predominantly in the cathodic field while the elastic type of fibrous tissue was produced predominantly in the anodic field.

In vitro production of radiating fibrous structures. In vitro demonstration of the outgrowth of radiating fibrous structures in a lung specimen depleted of air is difficult. However, it is informative to show that the same type of cathodic and anodic fibrous tissue that was produced in vitro in the rat lung can be produced also in vitro as radiating structures in fat tissue.

Normal human fat specimens obtained at herniorrhaphy or at mastectomy were used. A soft-tissue radiograph of a normal piece of human breast fat is shown in figure 25 in an electrophoretic chamber between two platinum electrodes provided with small protrusions. These are intended to produce electrical edge enhancement. The fat specimen contains some minor fibrous tissue elements before the application of current. After application of current (25 C at 10 V), new coarse radiating structures can be seen in the cathodic part as well as some more-irregular newly formed structures and many small "dots" in the anodic part of the specimen (fig. 25).

Histologic examination of the specimen (fixed in formaldehyde, sliced and stained with van Gieson stain) shows a meshlike fibrous material without any cell-like structures in

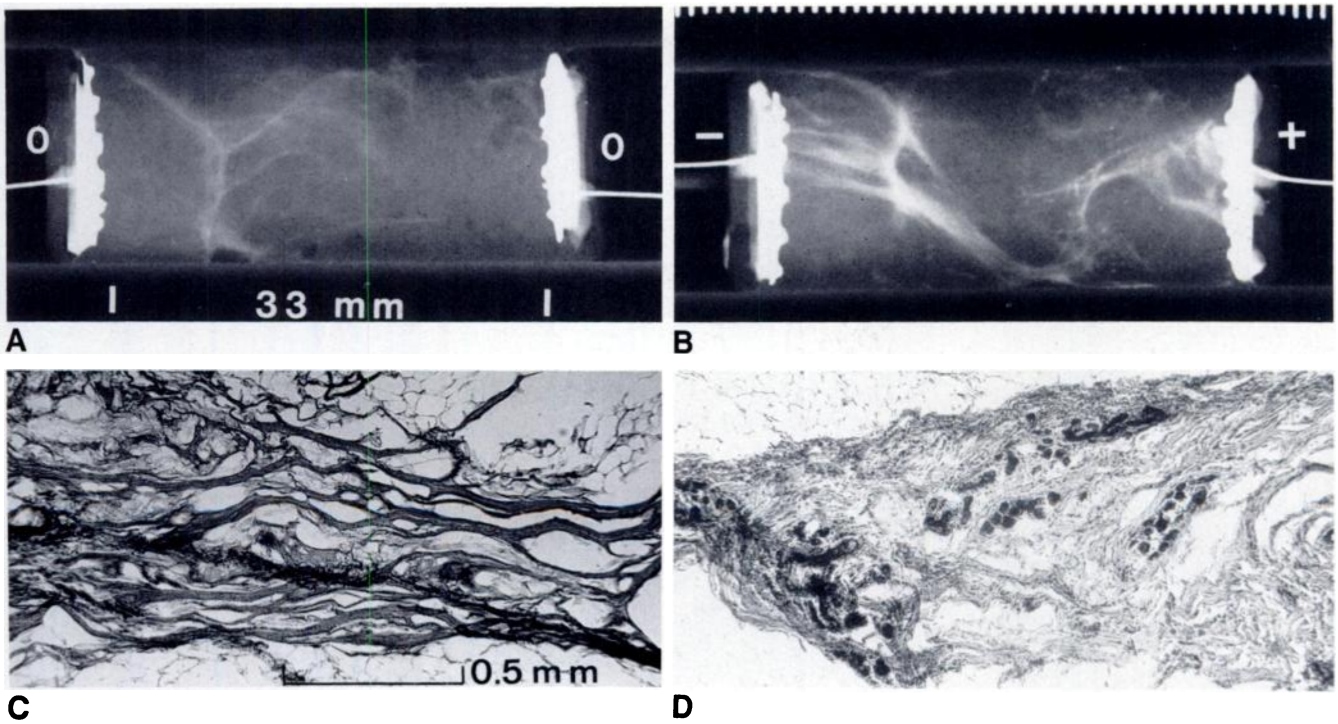

Fig. 25.—Induction of fibrosis in human fat tissue in vitro. Human breast fat in plastic chamber between two platinum electrodes with surface protrusions. **A**, Soft-tissue radiograph before electrophoresis. Virtually no fibrous tissue in parts of specimen adjacent to electrodes. **B**, After 10 days' application of 25 C at 10 V, radiating structures are produced owing to field enhancement at some of electrode protrusions. Note macroscopic differences between cathodic (−) and anodic (+) fibrous tissue as well as many small "dots" in anodic part of specimen. Histologic specimens: **C**, Meshlike cathodic fibrous radiating structures; **D**, dense, irregular anodic fibrous tissue, containing many fibroblastlike cells. (van Gieson stain.) (Reprinted from [2].)

the cathodic half of the specimen (fig. 25). In the anodic half (fig. 25), irregular fibrous material is seen with numerous celllike elements having the appearance of fibroblasts. On the whole, the types of cathodic and anodic fibrous tissues found in the treated human breast-fat specimen were similar to these in the treated rat lung lobe. Recent short-interval studies on the development of cathodic fibrous tissue in fat have revealed continuous thickening of fat cell membranes while nuclei and cytoplasm dissolve [2, pp. 236–240]. The anodic fibrous tissue seems to develop predominantly in the interstitial spaces and from cytoplasmic material. The fibroblastlike cells in the anodic tissue appear to consist of residual nuclei and cytoplasm from normal tissue cells.

Pure cathodic and anodic fibrous tissue cannot be expected to be found in normal scar tissue, because endogenously developed scar tissue (as well as the radiating fibrous structures around cancers) results from the fluctuating injury potential. Therefore, scar tissues in vivo contain a mixture of cathodic and anodic fibrosis (i.e., nonhygroscopic, collagenous, and hygroscopic elastic fibrous material).

In vivo production of radiating fibrous structures in human lung. Artificial activation of the VICC system in vivo is possible from an external source of direct current over implanted electrodes. Large amounts of energy can be supplied to the system, thus injuring the tissue and initiating an injury polarization potential [2, pp. 281–317]. When the application of external current is interrupted, the energy of the induced injury polarization starts the spontaneous repair of tissue. During this process radiating structures have been observed to develop.

Electrochemical treatment of a cancer provides an example. An adenocarcinoma of the ovary in a 66-year-old woman was partly excised, then treated locally with 4000 rad (40 Gy). Four years later, a 25 × 17 × 17-mm tumor appeared in the left lung. Needle biopsy confirmed the presence of an adenocarcinoma. Because the patient had coronary atherosclerosis, atrial fibrillation, and two myocardial infarctions, surgical resection was rejected. Instead, the cancer was treated electrochemically under local anesthesia over percutaneously applied platinum electrodes (figs. 26A and 26B) with 180 C at 10–15 V. The tumor was made anodic. Figure 26C shows the tumor before treatment. After 2 months, tiny radiating structures had appeared around the tumor as well as around a density above it, corresponding to the former position of the cathode (fig. 26D). Subsequently the tumor and the cathodic infiltrations decreased in size, still showing radiating structures (fig. 26E). Five years after treatment, only a minimal scar remained at the tumor site (fig. 26F).

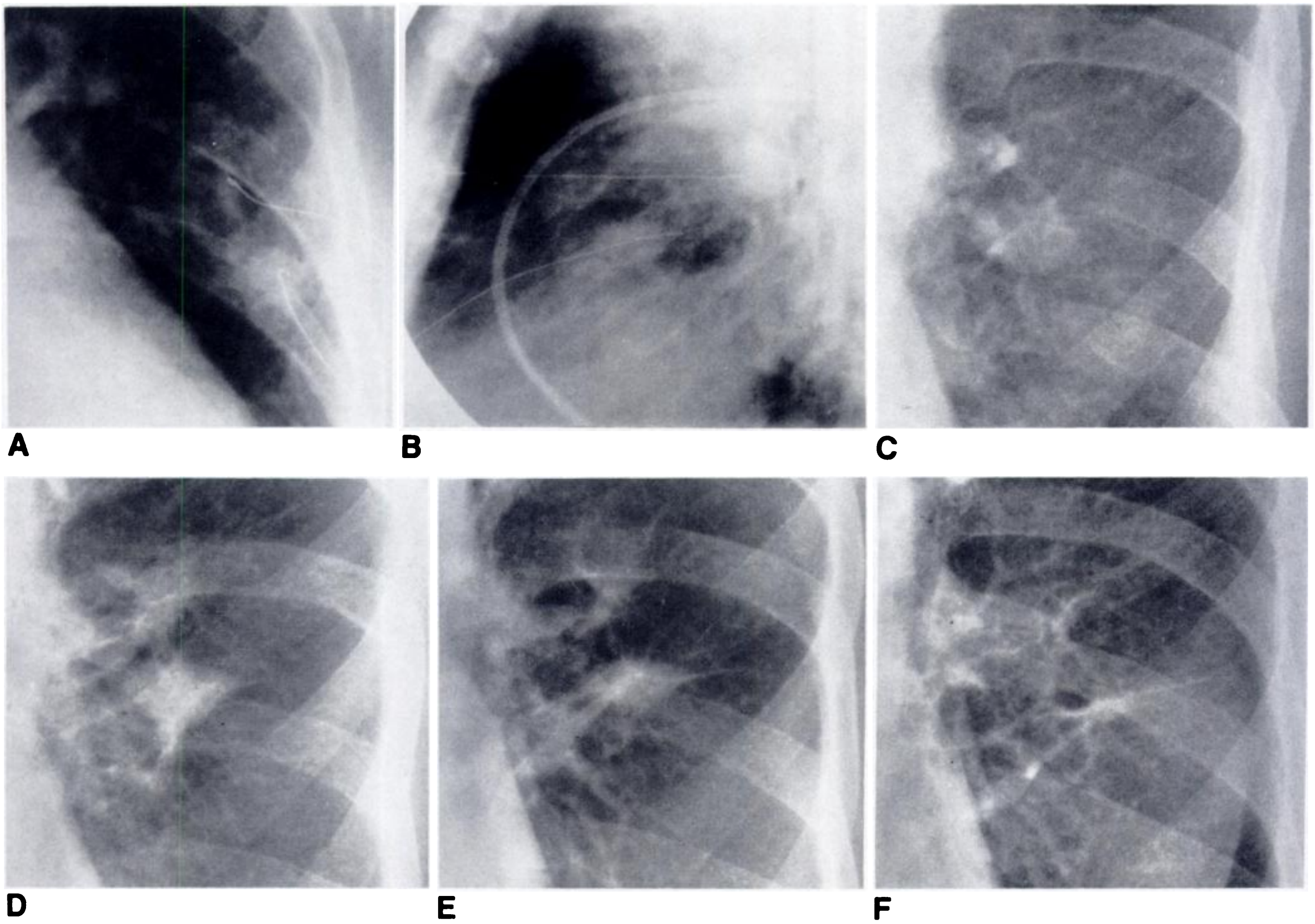

Fig. 26.—Production of fibrous radiating structures in vivo. Direct-current treatment of metastatic ovarian carcinoma in lingula of 66-year-old woman. Anteroposterior (**A**) and lateral (**B**) views show percutaneously inserted platinum electrodes in tumor (anode) and in lung tissue above tumor (cathode). An angiographic catheter is positioned in pulmonary artery. Radiographs before (**C**) and 30 days after (**D**) treatment with 180 C at 10–15 V show fibrous radiating structures around tumor and around former site of cathode. **E**, 60 days after treatment, tumor is smaller but radiating structures are still evident. **F**, After 450 days. Only a small focus of scar tissue remains at tumor site. Minimal fibrosis is present at former site of cathode. (**A–E** reprinted from [2].)

Retraction of Fibrous Tissue

A variety of factors are involved in retraction of tissue. Within an A zone, deterioration of the vascular supply may lead to true perifocal emphysema and the circular displacement of vessels. The surrounding normal tissue retracts from the now more compliant emphysematous region. A reversible type of tissue retraction is produced by tissue containing hygroscopic, fibrous, elastic tissue. Depending upon the water content, this tissue will either shrink or enlarge. The mechanism is involved in the development of "retraction pockets" in the lung with local accumulation of fluid in the adjacent pleural space.

Let us excise a piece of fibrous radiating scar tissue from the periphery of a breast cancer and divide it into two parts. Each is refrigerated overnight, one part soaked in saline solution and the other air-dried. Microscopic sections are then prepared. The soaked material shows straight birefringent collagenous fibers (fig. 27A). The birefringent fibers in the dried material are undulating owing to shrinkage of the elastic hygroscopic fibers between the birefringent fibers (fig. 27B).

A pulmonary lesion near the surface of the lung may produce what pathologists often call a "naveling" of the pleura. A small adenocarcinoma close to the chest wall is shown in figure 28A. Its surface is slightly irregular, with a fibrous strand suggested between the tumor and a tent-shaped pleural density. After operative resection, the radiograph of the inflated specimen revealed multiple small radiating structures at the surface of the tumor (fig. 28B). Some of these structures were attached to the visceral pleura, which shows naveling. The pleural tent-shaped density evidently was caused by in vivo collection of fluid in a retracted part of the visceral pleura.

The pathogenesis of this condition may be described as follows: A pulmonary lesion with an irregularly protruding surface, located near the pleura, may develop radiating fibrous

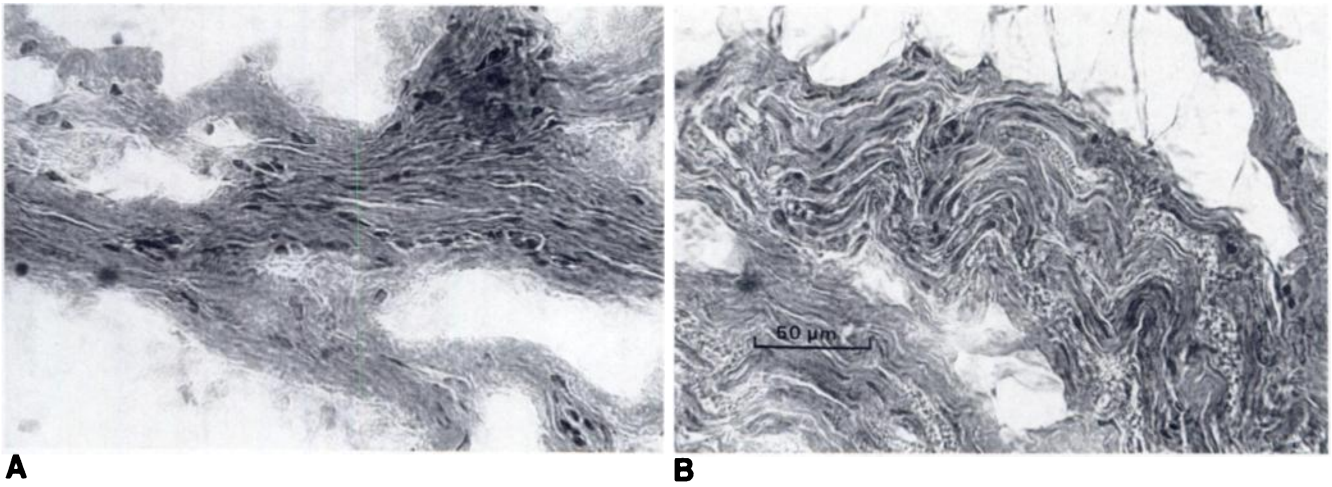

Fig. 27.—Modification of fibrous tissue by alteration of water content. Two specimens of fibrous tissue from breast cancer, after overnight refrigeration. One specimen was soaked in saline solution, the other exposed to air. After cutting and staining with hematoxylin-eosin, the soaked material (**A**) shows straight birefringent collagenous fibers; the dried material (**B**) shows undulating birefringent collagenous fibers. Undulations follow retraction of elastic, hydrophilic fibrous material between collagen fibers. (Reprinted from [2].)

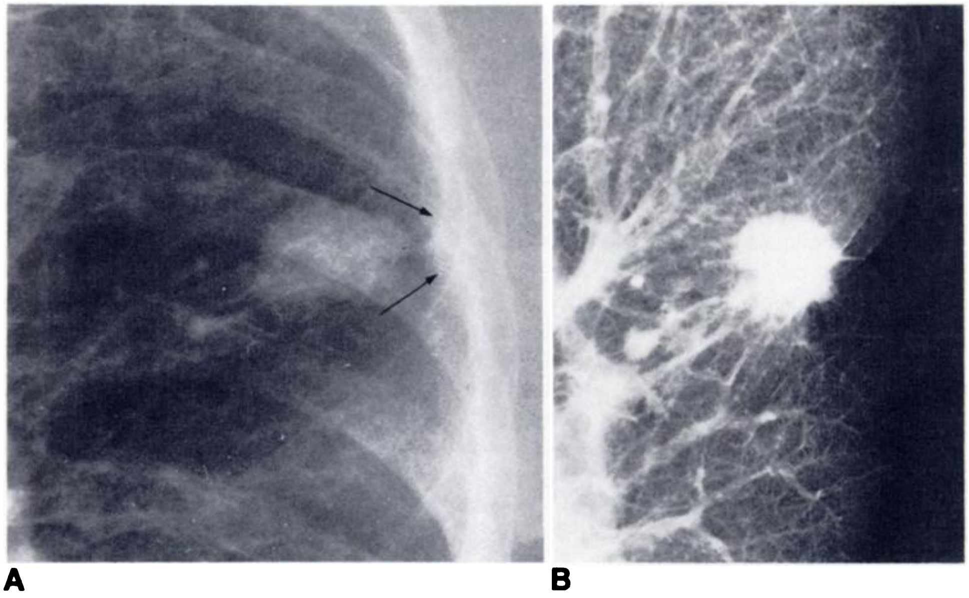

Fig. 28.—**A**, Pleural retraction pocket (*arrows*) adjacent to small adenocarcinoma in left upper lobe. B, Postmortem radiograph of lung, distended by negative external pressure, shows numerous small, radiating fibrous structures around tumor. One of these structures reaches pleura, which is retracted to a funnel (filled with pleural fluid in vivo). (Reprinted from [2].)

structures as described previously. Some of these extending structures may attach to the visceral pleura. During an electropositive phase of polarization of the tumor (by internal injury), a hydropenic zone will develop around the tumor. The hygroscopic fibrous elements of already developing radiating structures will then shrink and produce naveling of the pleura. This naveling is here called a retraction pocket. An analogous mechanism applies in the breast to the development of so-called skin retraction and skin thickening in the vicinity of a breast cancer. Quantitative analyses of relative fat-water content in the tissues have supported this concept [2, pp. 228-232].

Differential diagnosis between a B zone, thickened pleura, and a retraction pocket can be obtained by the injection of a small amount of air into the pleural space (fig. 29). These considerations are of practical importance because not all pleural reactions adjacent to cancers mean malignant involvement of the pleura.

Calcifications

Pathologic calcifications in human tissues consist of hydroxyapatite. This compound is a mixture of calcium, phosphate, carbonate, magnesium, variable amounts of water,

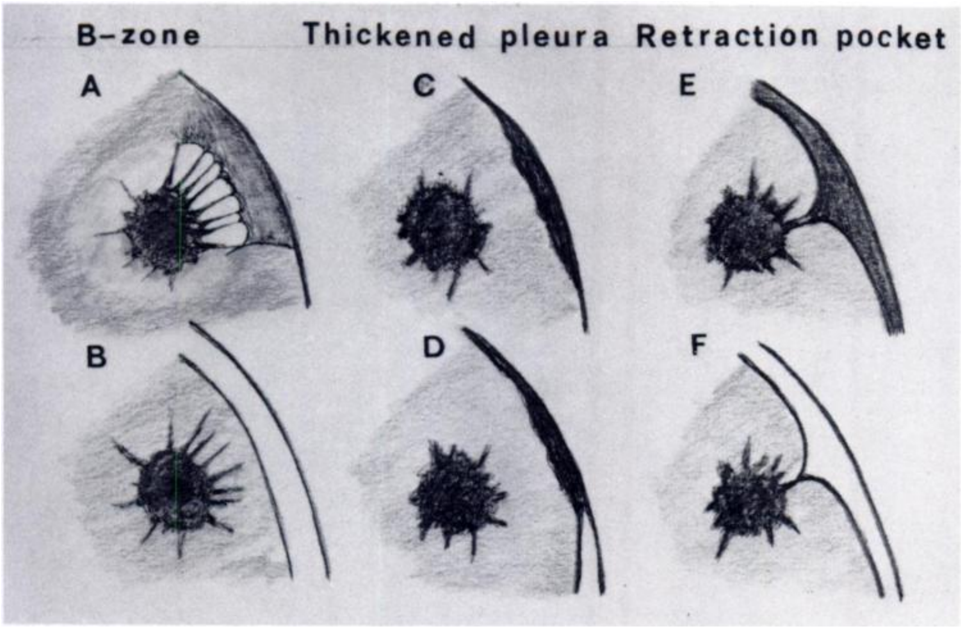

Fig. 29.—Schematic guide to differential diagnosis of B zone (**A**), thickened pleura (**C**), and pleural retraction pocket (**E**): With injection of small quantity of air into pleural space, B zone disapears (**B**); pleural thickening (**D**) and retraction pocket (**F**) remain. (Modified from [2].)

and "impurities" (e.g., protein). Apatite precipitates in any tissue after various kinds of injuries. By applying the principle of the fluctuating injury potential [2, pp. 69–73] and its activation of the VICC system, it is possible to give a general tentative explanation of the biokinetic events associated with calcification of tissue.

Microcalcifications in a specimen of adipose tissue from a human breast can be produced experimentally in vitro (figs. 30A and 30B). As a result of the flow of current through a tissue specimen, small radiopaque "dots" develop in the anodic part. Histologically, these dots correspond to bushlike, partly birefringent, structured material on the inside walls of fat cells (fig. 30C). These "bushes" do not contain chemically detectable calcium, an understandable phenomenon in that they have developed in the acidic environment of the electropositive (anodic) part of the specimen. However, the bushes represent a matrix, which seems to be a necessary prerequisite for the precipitation of calcium.

After the direct-current treatment of fat specimens resulted in the development of radiographically visible anodic "dots," the polarity was reversed, thereby simulating the events of a "fluctuating injury potential." Subsequent histologic analyses then revealed multiple foci of microcalcifications, which showed typical staining for calcium by hematoxylin-eosin (figs. 30D and 30E) and alizarin, which is specific for calcium ions.

In vivo induction of calcium accumulation in a human lung metastasis. The low-density tumor shown in figure 31A represents a cytologically verified metastatic melanosarcoma in the left lung of a 32-year-old woman. This tumor was electrocoagulated by diathermy over an active electrode perfused by saline solution [2, pp. 273–281]. The temperature measured at the periphery of the tumor rose to 50°–60°C after about 8 min. Two months after the treatment, the tumor appeared more radiopaque than adjacent ribs (fig. 31B). This finding could be interpreted only as the result of accumulation of calcium in the injured tissue. Six months after treatment, the tumor had diminished considerably and showed a calcium-dense area only in its central region (fig. 31C).

Clinical observations of electrochemical treatment of cancers of the lung as well as the production of microcalcifications in in vitro experiments indicate that calcifications in tissue need not necessarily be regarded as a disease per se. In my opinion, many so-called pathologic calcifications in previously injured tissue represent a process that can be regarded pathogenetically as equivalent to the development of scar tissue. This process behind injury-induced tissue calcifications may therefore be termed *calcinosis reparativa*, to indicate its close relation to the events of healing.

Comment

The role of the VICC system is described here mainly in terms of the development of radiographically visible structures in spontaneously degrading pulmonary lesions. From observations detailed elsewhere, analogous correlations exist concerning endogenous transformations of tissue in degrading breast cancers [2, pp. 203–268]. It is suggested that an activated VICC system also leads to many other physiologic and pathophysiologic events.

For example, an energetically acceptable explanation for chemotaxis [2, pp. 191–192] is now possible in terms of endogenous electrophoretic transport of charged materials. White blood cells, which are electronegatively charged, were shown to accumulate massively around an electropositively polarized tissue region [2, pp. 187–191]. In this sense, leukotaxis may be explained as endogenous in vivo electrophoresis of white blood cells.

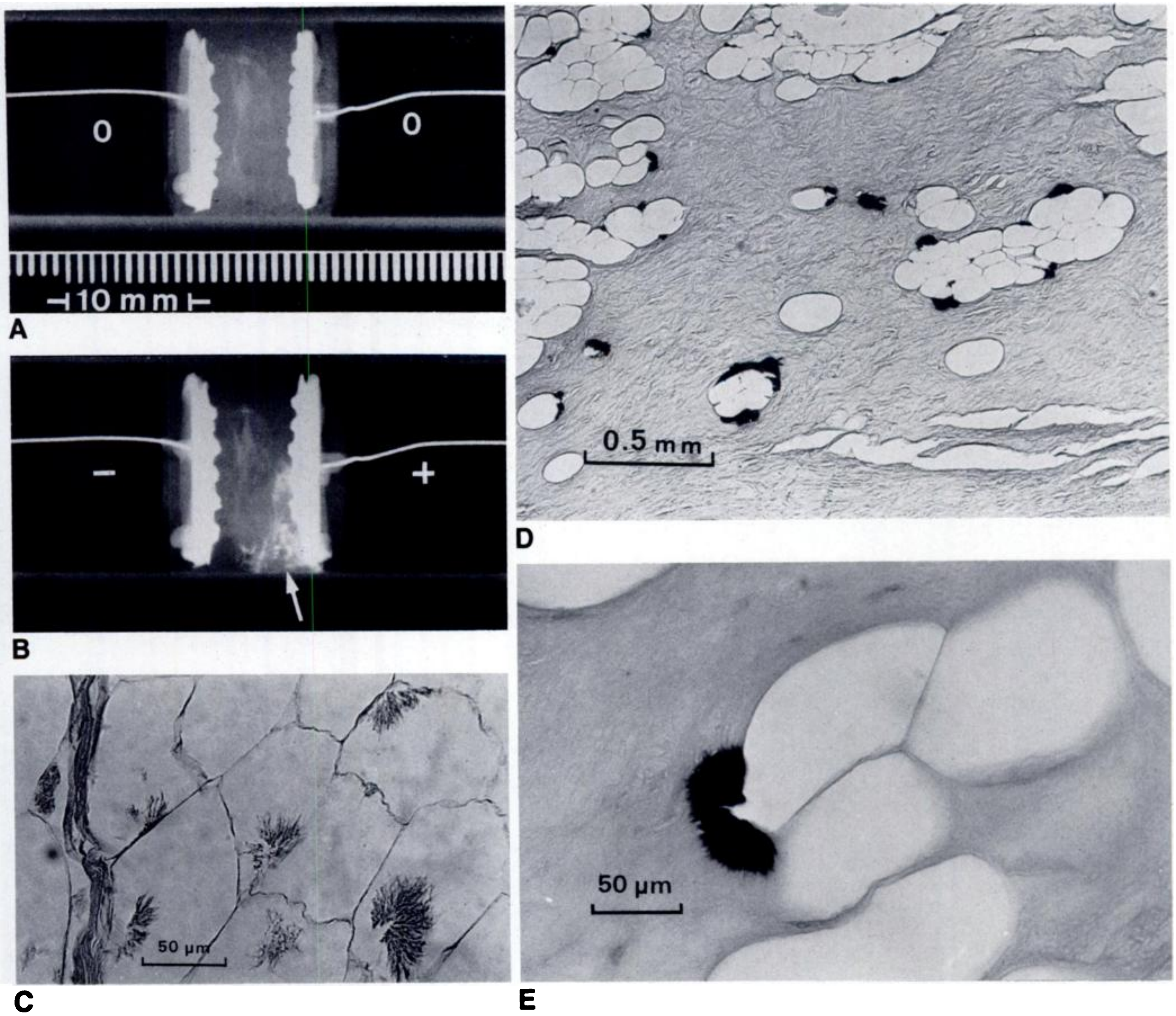

Fig. 30.—Creation of microcalcifications in normal breast fat in vitro. **A**, Soft-tissue radiograph of electrophoretic chamber containing fat specimen before application of direct current. **B**, After 25 C at 10 V (26 days), small "dots" are seen in lower part of anodic field (*arrow*). **C**, Photomicrograph (hematoxylin-eosin) of "dots," bushlike structures that developed on inner membrane of fat cells. At this stage, these anodic matrices contain no calcium. Flow of current was then reversed, simulating endogenous fluctuation of an injury potential; previously anodic "dots" (matrices) then calcified. Subsequent histologic specimen (**D**) shows scattered microcalcifications in previously radiographically normal, noncalcified tissue. (**E**, Detail of microcalcification.) (H and E stain.) (**A–C** reprinted from [2].)

"Local" chemical reactions will be modified, insofar as they occur within superimposed VICC-mediated electrochemical gradients among various metabolically polarizing tissue regions. The VICC system can thereby be expected to play an important role in maintaining homeostasis.

Physiologic modulations by the VICC system may also be turned into unphysiologic activations, however, leading to pathologic transformations of cells. Thus, hybridization of red blood cells and fat cells into monstrous cell-like units have been produced experimentally [2, pp. 183–186]. An unphysiologic, long-term, unidirectional activation of the VICC system may therefore represent a hitherto unrecognized mechanism for the induction of neoplasms by the various electrochemically tissue-polarizing agents among carcinogens [2, p. 327].

On the other hand, it is possible to induce dramatic changes of the ionic microenvironment of various cancers when the VICC system is acutely overstimulated via implanted electrodes from an external source of direct current. This process already has led to apparently permanent (now of 6 years' duration) regression of a number of seemingly uncontrollable cancers [2, pp. 269–317].

It seems justified to suggest that the VICC system may represent an important mechanism to consider in future at-

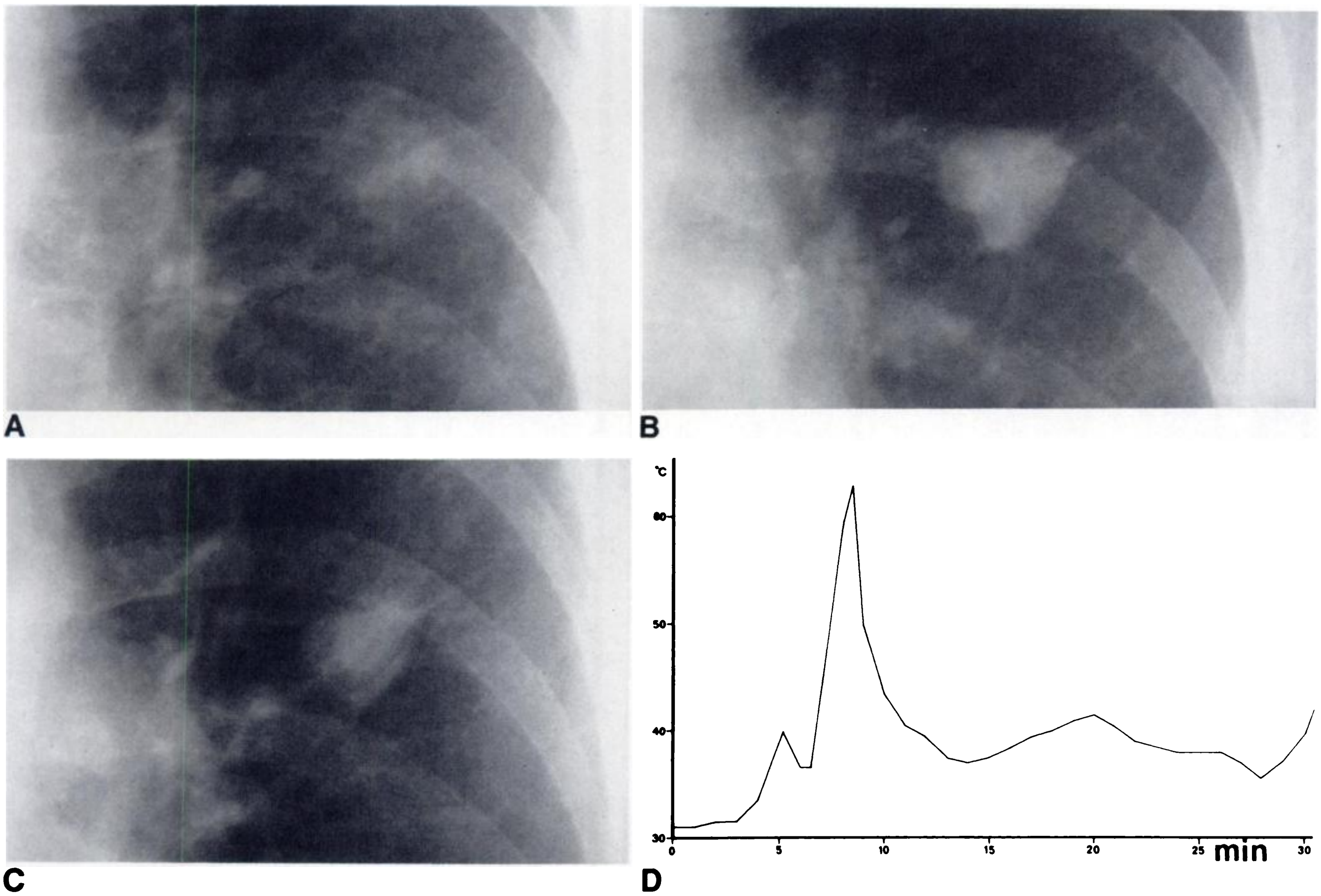

Fig. 31.—Induction of calcification in metastatic melanosarcoma by electrocoagulation. **A**, Original low radiographic opacity. **B**, 60 days after treatment, tumor appears even more opaque than surrounding ribs. **C**, 180 days after treatment, tumor has diminished considerably. Increased radiopacity probably represents inflow of calcium into injured tumor tissue. **D**, Temperature measured at tumor during electrocoagulation. (Reprinted from [2].)

tempts at explaining various functional and morphologic biologic phenomena that are now poorly understood. Further investigation of the construction and function of the VICC system also seems justified, as it may offer new possibilities for influencing the healing of various disorders of tissues and cells.

ACKNOWLEDGMENTS

I thank John H. M. Austin for help in preparing the English text and Kerstin Ersson for help in manuscript preparation.

REFERENCES

1. Nordenström BEW. New trends and techniques in roentgen diagnosis of bronchial carcinoma. In: Simon M, Potchen EJ, Le May M, eds. *Frontiers of pulmonary radiology*. New York: Grune & Stratton, **1969**:380–404
2. Nordenström BEW. *Biologically closed electric circuits: clinical, experimental and theoretical evidence for an additional circulatory system*. Stockholm: Nordic Medical Publications, **1983** (available through Nordic Medical Publications, Grev Turegatan 2, S-114 35 Stockholm, Sweden)
3. Nordenström BEW. Electric potentials in pulmonary lesions. *Acta Radiol* [*Diagn*] (Stockh) **1971**;11:1–16
4. Jordan J. In: Pilla AA, ed. *Proceedings of a workshop in bioelectrochemistry, Princeton, New Jersey, October 10–14, 1971.* Washington DC: National Science Foundation; and Yardley, PA: ESB, Inc. Technology Center, **1971**:103–122
5. Weiss L, Zeigel R. Cell surface negativity and the binding of positively charged particles. *J Cell Physiol* **1971**;77:179–186

Editor's Note

Several aspects of the publication of this lecture are unconventional and require explanation. The work is unique in more than its intriguing content. Unlike the multiauthor contributions that dominate today's literature, every aspect of this offering is solely from one man, Professor Nordenström. Having worked without collaborators for over a decade, he alone is responsible for the original concepts, the experiments, the analysis, and the text. Although employing modern terms and instruments, his performance has been in the tradition of the pioneer scientist: complete and isolated immersion in the research. There can be no doubt as to whom the ingenious experiments and ground-breaking conceptions should be credited.

The manner of publication of this work is also unique. Only two papers on the subject have been offered in the public domain. Rather, the entirety of the effort has been laid out in great detail in a recently published volume [2]. Although Professor Nordenström has spoken about some of the material at international gatherings, the bulk of it has not been available in print for others to contemplate and assess. Accordingly, there has been little correlative investigation in other laboratories. Few, if any, of the experiments have been replicated; as a result, the concepts, though plausible, have not had the advantage of independent supportive investigation elsewhere. Reviews of the work by other scientists familiar with the concepts and techniques have not yet been possible. Thus, the lecture is offered to our readers without the conventional external assessment.

This seems justified on the basis of the solid science in Professor Nordenström's many preceding contributions to radiology. Further, the relevance to diagnostic images is very pertinent as details of these are conventionally explained exclusively on a histopathologic basis. Many of the concepts presented will be unfamiliar to radiologists, and more than one reading may be required for a comfortable grasp of the numerous interrelated ideas that offer seemingly plausible explanations for many pathologic and radiologic phenomena. Some may object that this largely theoretical work has no place in a journal which carries predominantly practical clinical information. Yet, how can the regression of lung tumors as a consequence of electrical treatment be other than clinical and practical, at least to the individuals concerned?

It is too early to offer final judgment of this work. At the very least it is imaginative, experimentally ingenious, and provocative. Professor Nordenström has raised many tantalizing questions. Space limitations prevent full exposition, which might answer some of them, but even so, other questions would still remain. Clearly the work calls for similar investigations elsewhere; it is hoped that this publication will encourage such efforts. Professor Nordenström's book contains a wealth of experimental details for those who may be so stimulated. Like this paper, it is phrased with some dogmatism and certainty; nevertheless, it is a collection of many intriguing hypotheses that warrant serious examination. Possibly these new concepts are our first realization of an important physicochemical system that heretofore has been overlooked. If so, Professor Nordenström would take his place with other notable Swedish scientists who have so greatly advanced our understanding of electrophysiology and biophysics.

MMF